Surface Chemistry of Low-Dimensional Carbon Materials:
Synthesis and Functionalization of Graphene

Dissertation zur Erlangung des akademischen Grades des Doktors der Naturwissenschaften (Dr. rer. nat.)

vorgelegt von

Guy Guday

aus Jerusalem

Institut für Organische Chemie

Fachbereich Biologie, Chemie, Pharmazie

Freie Universität Berlin

August 2019

Declaration of honesty

I hereby declare that this PhD thesis is entirely the product of my own work. No other sources have been used other than those cited. All figures and schemes have been created by me or have been properly identified with the corresponding references.

Guy Guday

Berlin, 30.06.2019

The following project was carried out within the research group of Prof. Dr. Rainer Haag from January 2016 until August 2019 at the Institute of Chemistry and Biochemistry of the Freie Universität Berlin.

1. Reviewer: Prof. Dr. Rainer Haag, Freie Universität Berlin

2. Reviewer: Prof. Dr. Mohsen Adeli, Freie Universität Berlin, Lorestan University

Day of defense: 11.09.2019

Acknowledgements

I would like to first thank Prof. Dr. Rainer Haag for the chance to join and be a part of his group. His support and guidance over the course of my work has been instrumental and cannot be understated. The financial support across multiple channels that he was able to arrange has been greatly appreciated as well.

I would also like to thank Prof. Dr. Mohsen Adeli for his hands-on guidance through the challenges of working with graphene. He has been a mentor and a source of inspiration throughout my work and has offered advice and guidance as well on my new role as a father, and how to balance both of those worlds.

Furthermore, I would like to thank all the colleagues and collaboration partners who I have had the distinct pleasure to work with and learn from. Ievgen Donskyi, Mohammed Fardin Gholami, Dr. Gerardo Algara-Siller, Felix Witte, Prof. Dr. Beate Paulus, Prof. Dr. Jürgen Rabe, Abbas Faghani, Zhaoxu Tu, and Philip Nickl. Without their help and participation, many of these projects would not have been successful.

All of the current and previous members of AG Haag have been friends and supporters, offering scientific expertise and experience as well as friendship and support through all of the highs and lows of life as a doctoral student. In particular the members of the Carbon Subgroup, Prof. Dr. Chong Cheng, Rameez Ahmed, and Vahid Ahmadi. Also Dr. Luis Cuellar who helped train me on the AFM and troubleshoot challenging samples, Dr. Mathias Dimde for his help with nanogel systems, Dr. Olaf Wagner for his helpful suggestions and the material needed for fluorous experiments.

I would also like to highlight my colleagues in Arnimallee 22, Dr. Zewang You, Anna Herrmann, Michaël Kulka, and Rotsi Randriantsilefisoa, who joined us in our exile. We have all helped each other to turn Arnimallee into a livable and enjoyable working space, and for their roles in making life nicer and more fun, I am eternally grateful.

I am thankful for the entire support staff of AG Haag works tirelessly to enable all of us to conduct our research with as few limitations and challenges as possible.

Dr. Wiebke Fischer and Eike Ziegler have been my main contacts for everything administrative, helping with documentation for funding, travel, submitting our

manuscripts, and everything in between – including helping set up and organize group events that all of us are able to enjoy.

The Technical Staff who keep all our shared equipment running, conduct experiments and measurements on our behalf, synthesize polyglycerol ceaselessly – and much more – will never know just how much easier our jobs are thanks to theirs.

Finally, I am thankful for the love and support of my family and friends, most especially my wife and daughter. I started down this path alone, out of a passion and interest in chemistry and materials science. I continue in my life now with both of them by my side, always helping me push forward through thick and thin. Love is impossible to quantify and difficult to describe – like much in this scientific realm, as well – but it is remarkably easy to show, to see, and to feel. I hope that I have always remembered to offer the same love in return that they have given me unconditionally.

List of Abbreviations

0D	Zero-dimensional
1D	One-dimensional
2D	Two-dimensional
3D	Three-dimensional
AA	Acetic acid
APTS	3-aminopropyltriethoxysilane
ATRP	Atom transfer radical polymerization
ATS	Azidotrimethyl silane
CNT	Carbon nanotubes
CH	Chitosan
CS	Coronene tetracarboxylic acid
CVD	Chemical vapor deposition
DA	Diels-Alder
DBC	Dibromocarbene
DMAEMA	N,N-dimethylaminoethyl methacrylate
DMF	Dimethyl formamide
DMPG	1,2-Dimyristoyl-sn-glycero-3-phosphoglycerol
DMSO	Dimethyl sulfoxide
DOX	Doxorubicin
EG	Thermally exfoliated graphene oxide
EPR	Enhanced permeability and retention
FTIR	Fourier transform infrared spectroscopy
fTPP	Fluorinated triphenylphosphine
GO	Graphene oxide
GPa	Gigapascal
HG	Arc evaporated graphene, produced under hydrogen atmosphere
HOMO	Highest occupied molecular orbital
HR-TEM	High-resolution transmission electron microscopy
LUMO	Lowest unoccupied molecular orbital
NEXAFS	Near-edge X-ray absorption fluorescence spectroscopy
nG	Nanographene
NGO	Nanographene oxide
nGTrz	nG modified with 1-azido-3,5-dichloro-2,4,6-triazine

nGTrz-PF	nGTrz post-modified with perfluoroalkanes
nGTrz-PF-fTPP	nGTrz-PF loaded with fluorinated triphenyl phosphine
NIR	Near-infrared radiation
nm	Nanometer
NMR	Nuclear magnetic resonance
PEG	Poly(ethylene glycol)
PF	Perfluoroalkane
Ph	Phenyl group
PLL	Poly-l-lysine
PNIPAM	Poly(n-isopropyl acrylamide)
PS	Polystyrene
PVA	Poly(vinyl alcohol)
QD	Quantum dot
RGO	Reduced graphene oxide
SFM-PFTUNA	Scanning force microscopy PeakForce Tunneling
SFM-TM	Scanning force microscopy in tapping mode
SIPGP	Self-initiated photografting and photopolymerization
TEMP-MI	N-(2,2,6,6-tetramethyl-piperidinyl)-maleimide
TEMPO-MI	N-(1-oxyl-2,2,6,6,-tetramethyl-4-piperidinyl)-maleimide
Trz	2-azido-4,6-dichloro-1,3,5-triazine
UV	Ultraviolet
XPS	X-ray photoelectron spectroscopy

Table of Contents

1 Introduction

1.1 Conjugated Carbon Allotropes

Carbon is one of the fundamental building blocks of life on Earth. In its elemental form, there are a range of possible structures, or allotropes, that can be found or produced. Graphite is a naturally occurring crystalline and conjugated form of carbon. Man-made carbon allotropes (Figure 1.1) have become increasingly important, as even subtle variations in their conformation and structure can yield wildly different properties, especially when comparing carbon nanomaterials. Graphite, most widely recognized as pencil lead, is structurally similar to graphene – indeed, graphene can be prepared by peeling apart graphite into the single layers that are stacked together to comprise its structure. However, one is a strong[2-4] material with exceptional thermal and electronic conductivity[5-8] and a range of unique electro-optical properties[6,9-12] while the other exhibits only limited conductivity[13-14] and, as a bulk material, is used as an industrial dry lubricant. While a host of additional rare or exceptional carbon allotropes exist, the ones that will be discussed here are the more common carbon nanomaterials – fullerenes, carbon nanotubes (CNTs), and the graphenic materials, graphene oxide (GO) and graphene.

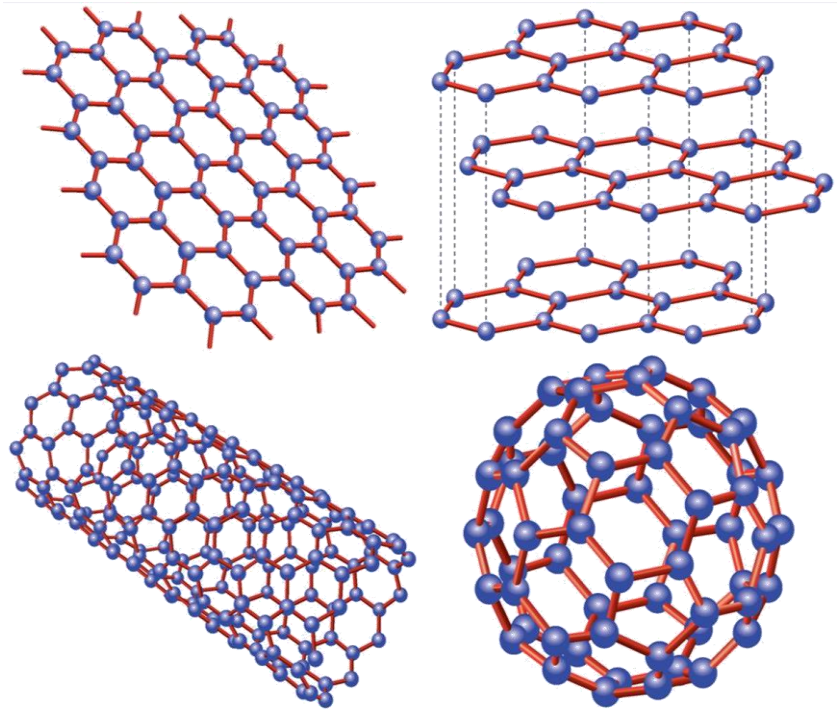

Figure 1.1. Low-dimensional carbon allotropes. Clockwise from top left: monolayer graphene, multilayer graphene, C_{60} fullerene, and carbon nanotube (CNT). Figure taken from *Physics* World November 2006 p36.[1] Reproduced with permission of IOP Publishing

1.1.1 Fullerenes

Fullerenes are a class of carbon spheroids often approximated to be 0D carbon nanomaterials, most commonly typified by the C_{60} "buckyball".[15] The structure is reminiscent of a soccer ball, with 20 hexagonal and 12 pentagonal rings. All of the carbons in a buckyball are sp^2 hybridized, a shared trait across all of the carbon nanomaterials in this chapter.

Fullerenes are the longest studied of this class of material, having first been discovered in 1985, for which the 1996 Nobel Prize in Chemistry was awarded.[15] Since then, fullerenes have been extensively studied. These nanoparticles behave as quantum dots (QDs), exhibiting both particle- and wave-like properties.[16] As a result, a number of interesting and potentially useful optical properties arise, such as fluorescence.[17-19] Most fullerenes, including buckyballs, are inherently electronic insulators, as they do not exhibit superaromaticity, meaning the π electrons are not delocalized across the entire aromatic network.[20-21] Fullerenes are also strongly hydrophobic,[22] which is easily understood when considering that fullerenes are largely comprised of interconnected benzene rings, and benzene itself is hydrophobic.

A major area of research interests has been the covalent or non-covalent modification of fullerenes, as a way to tune and modify their properties.[23-25] Functionalities have been added in order to solubilize fullerenes in aqueous systems,[22,26-29] alter conductivity or charge carrier capacities,[27-28,30-33] or enable or improve drug loading and targeted therapies,[22,27-29,34-35] amongst other applications. While fullerenes are generally quite stable, they are still reactive, due in large part to their curvature. The six-membered sp^2 rings of fullerenes prefer a flat planar conformation, leading to higher reactivity, especially at 6,6 carbon centers. These centers will react comparatively easily to form sp^3 carbons, alleviating some of the bond strain inherent to the native fullerene structure.[23-24,36-37] In fact, most methods for the functionalization of low-dimensional carbon nanomaterials were pioneered with fullerenes, before applications with nanotubes and subsequently with graphene were explored.

1.1.2 Carbon Nanotubes

If fullerenes may be thought of as 0D carbon nanomaterials, CNTs are their 1D cousins. The tubes consist of tessellated benzene rings, rolled around one axis and linear in an orthogonal axis. CNTs can be produced as single tubes or as concentric arrangements with multiple layers.[38-39] CNTs are inherently chiral, as the tessellation of rings along the tube can follow different and very specific twisting patterns.[21,40] These various conformations exhibit distinct and sometimes drastically different properties, making CNTs perhaps the most diverse set of carbon allotropes.

As might be expected, CNTs share many similarities with fullerenes. CNTs are also optically active and fluorescent,[39,41] and are mechanically quite strong. In tension, CNTs have demonstrated elastic moduli on the order of 100 GPa,[42] making them one of the strongest known materials. However, due to their extremely high aspect ratio – a length that is much higher than diameter – CNTs tend to be relatively weak under compression, torsion, or bending. CNTs can exhibit one of three broad electronic behaviors, depending on the orientation of their twisting: metallic, quasi-metallic, or semi-conducting.[21,40] It is important to note, however, that CNTs are only highly conductive along their longitudinal axis. Due to their small diameters and highly curved sides, lateral conduction is quite low.

As with fullerenes, surface modification of CNTs has been a major topic of research since shortly after their initial discovery, and for many of the same reasons.[43-46] CNTs have shown an exceptional potential for tuning of electrooptical properties, including band gap modification[47] and absorption and luminescence or fluorescence.[39,48-51] CNTs have also been functionalized to improve solubility or biocompatibility, and enable targeted drug delivery and combination therapies.[41,46,48,50,52-58] With their curved structure, CNTs also exhibit strain-enhanced reactivity, which is also dependent on the diameter and twisting orientation of the CNT.

1.1.3 Graphene and Graphene Oxide

Graphene and graphene oxide (GO) are closely related 2D carbon allotropes. Interestingly, GO is also the oldest carbon nanomaterial to be produced, as early as 1859, although the true 2D nature of the material was first realized much later.[13,59-60] GO is derived from graphite by oxidation with sulfuric and nitric acid along with potassium permanganate. The resulting graphite oxide can then be exfoliated to yield GO, an amphiphilic 2D sheet that retains many sp^2 hybridized, six-membered carbon rings, but does introduce a large number of sp^3 oxo-defects.[61] Hummer's method remains the most common route towards producing graphenic materials, though slight modifications and improvements have been added over the last 60 years.[13-14,62-63] Graphene, meanwhile, was first produced in 2004 by exfoliating unmodified graphite using Scotch tape, [5] though more recent methods include chemical vapor deposition (CVD),[6,64] liquid solvent exfoliation,[65-67] and bottom-up organic synthesis (Figure 1.2).[68-69]

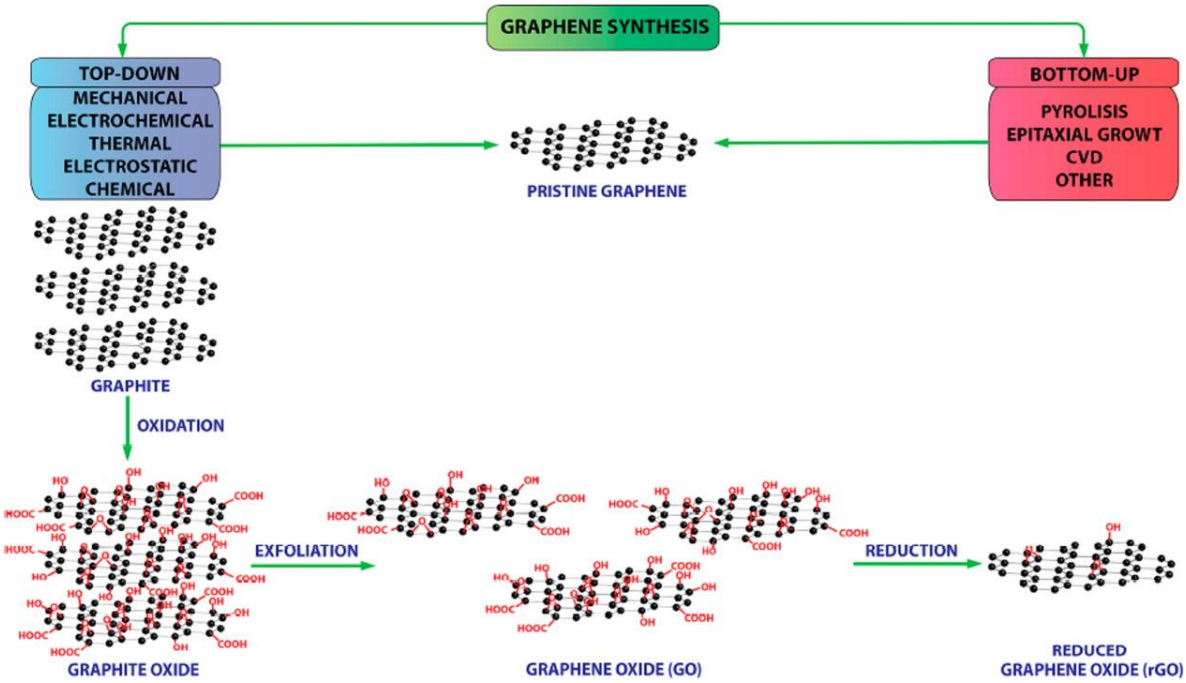

Figure 1.2. General scheme for the most common routes of graphene and graphene oxide synthesis. Reproduced with permission.[70] Copyright 2018, Wiley and Sons.

GO contains a large number of oxygen-based functional groups, namely carboxyls, hydroxyls, and epoxies, formed by the harsh oxidative conditions of preparation.[60] These groups are not homogeneously distributed across the sheets, though. Carboxylic groups are found primarily at or near the edges of the sheets, and epoxies mostly in the basal plane, while hydroxyl groups are generally found across the entire sheet.[71-72] These functionalities can be beneficial for some applications, as they are useful for both non-covalent and covalent conjugation of additional molecules. Carboxylic groups can for instance be modified by many common organic reactions. While GO does retain many unmodified hydrophobic rings in its basal plane, the oxygen groups lead to significant differences in the properties of GO as compared to pristine graphene.

GO is generally dispersible in water thanks to the hydroxy and carboxylic groups decorating it, whereas graphene aggregates rapidly due to its hydrophobicity in concert with inter-sheet π-π stacking.[13,65-66] By correlation, while both GO and graphene can be non-covalently loaded with hydrophobic or aromatic compounds such as pharmaceuticals, increasing degrees of oxidation place a cap on the loading capacity, as less of the GO surface is hydrophobic or aromatic.[11,73-74] There is also a very complex interplay between sheet geometries and surface chemistry insofar as biological interactions are concerned. Unfortunately there is no consistent trend whereby either GO or graphene are more

biocompatible; each factor from the source materials, to the method of preparation, to the nature of the biological testing and the specific types of cells investigated can drastically change the results.[75]

Graphene is famously highly conductive, both electronically and thermally.[5-6,67] This electronic conductivity arises due to the superaromaticity of graphene sheets; that is, the π electrons are delocalized not only across each individual ring, but over the entire sp^2 domain of the sheet. Superaromaticity also clarifies why defects, such as the oxygen groups of GO, can interfere with and degrade electronic properties. The sp^3 carbons in the GO plane cannot participate in a delocalized aromatic system. As the concentration of defects increases, the size of uninterrupted sp^2 domains shrinks, and more barriers to the movement of electrons are formed.[76-77]

GO can be reduced via thermal or chemical means to produce reduced graphene oxide (RGO).[7,13,78-79] However, while these routes may remove oxygen defects, they do not restore sp^2 hybridization of those carbons at the defect sites. Most of these processes instead replace oxygen-containing functionalities with hydrogen or other functional groups. While this can restore hydrophobicity and even partially restore electronic conductivity and optical properties, there is still a large delta between pristine graphene and RGO materials.

1.1.3.1 Nanographenes

As an ever-increasing array of methods for producing graphene and graphene oxide are reported, the detailed distinctions and characteristics of the prepared materials becomes critical. After all, it is well-established that differences in the geometry – both laterally and in thickness – as well as surface chemistry of graphenic materials can drastically change the resulting sheets or platelets.[10-11,68,73,75,80-83] Properties as fundamental as magnetism,[84] electrical conductivity,[85-86] and other optoelectronic properties[87] begin to change rapidly as a function of size in this nanoscale regime. It is hardly a surprise then that the roles and interactions of different nanographenes vary widely in larger scale systems – from biological interactions[10,75,88-92] to orchestrated nanomechanical devices.[93-94]

Graphene and graphene oxide are broadly classified as nanosheets if their lateral sizes are significantly below 1 μm across.[68] However, within this range there are a number of very distinct smaller sizes and conformations which are noteworthy. Sheets around 10-100 nm in diameter are classed as quantum dots; in this range, unique properties begin to arise due to quantum confinement effects, such as fluorescence. Other optoelectronic properties also change and can be tuned based on size, including conductivity and band gap size.[68,87,95-96]

Quantum dots of both graphene and graphene oxide are generally prepared by taking larger graphene, GO, or CNTs and mechanically or chemically breaking them down into smaller pieces.[87,97-98] Graphene stripes with a width under 10 nm and a length at least 10 times greater than their width are termed nanoribbons. Graphene nanoribbons are generally prepared by longitudinally opening CNTs, a process that allows for comparably precise control of geometry thanks to the defined CNT starting materials. Graphene nanoribbons have shown exceptional promise for electronic applications where uniformity is often crucial.[68-69,92] Even smaller graphene fragments, sometimes referred to as graphene molecules, have lateral sizes of less than about 10 nm.[68-69] One reason for their name is that graphene molecules are synthesized from smaller starting compounds, for instance via dehydrative π-extension[86] or alkyne benzannulation.[99] While the products of these synthetic routes are still very limited in size, work is ongoing to expand, including the recent synthesis of increasingly complex 3D graphenic architectures[100] and graphene nanoribbons reaching lengths of nearly 8 nm.[101]

Unfortunately, the production of nanographenes is a game of balance and priorities. High-yield, scalable methods exist for the synthesis of nanographene oxides – namely through the mechanical or chemical degradation of larger GO or graphene sheets or even CNTs.[38,102-103] However, the oxidative nature of these reactions, coupled in many cases with already-oxidized nanomaterial precursors, result in highly oxidized NGO[38] and typically also shows a comparatively broad range of sizes within each batch –ranging from quantum dots into the hundreds of nm range.[103] Bottom-up growth of nanographenes can be achieved using carefully controlled CVD or other surface-mediated growth mechanisms, although yield is extremely limited, as the nanographene sheets can only be grown on 2D substrates.[8,64,104-105] Alternatively, organic synthesis of graphene molecules can exert careful and reproducible control over the resulting sheets. These synthetic techniques are especially promising for molecular electronics, though they are still quite limited in sheet size and geometry, as well as scalability.[68-70,85,99] There are a growing number of methods to straddle the boundaries and limitations of these methods, such as the direct treatment of graphite with hypochlorite and subsequent exfoliation into nanographene.[106] The produced sheets may not exhibit the precise control of graphene molecules, but are more monodispersed in size than other top-down wet chemistry routes. Furthermore, the degree of oxidation induced by the hypochlorite treatment is quite low, approaching that of CVD or epitaxially grown graphene materials. The size range is however very limited, as efforts to move to larger or smaller sheet sizes have not yet shown significant effects.

1.2 Functionalization of Graphene and Graphene Oxide

1.2.1 Non-Covalent Functionalization

Non-covalent functionalization of graphene materials is perhaps the easiest method to tune their surface chemistry. Most methods for covalent conjugation onto the basal plane of graphene or GO either require existing sp^3 defects or introduce new ones. These defects disrupt the integrated aromatic network of pristine graphene. Therefore, noncovalent modification of graphene is of great interest for applications where the aromaticity is crucial, and the limitations and drawbacks of non-covalent interactions are acceptable. These noncovalent interactions typically arise from a combination of π–π stacking, hydrophobic interactions, or electrostatic forces.

1.2.1.1 π–π stacking

π–π stacking can occur between molecules with aromatic systems, adhering them to one another. As the π system of graphene sheets extends across most or all of the sheet, it is easy to expect that such interactions can non-covalently bind functionalities onto the surfaces of graphene sheets. π–π stacking of aromatic amphiphiles can even overcome the internal cohesion of layers within graphite powder, enabling exfoliation of individual sheets due to the hydrophilic tails of these exfoliating agents.[107] While GO sheets display significantly reduced π-π interactions due to the relative loss of aromatic rings, RGO sheets seem to regain loading capacity for non-covalently bound molecules, including chiral mesogenic molecules [108] and multiple pyrene derivatives.[109]

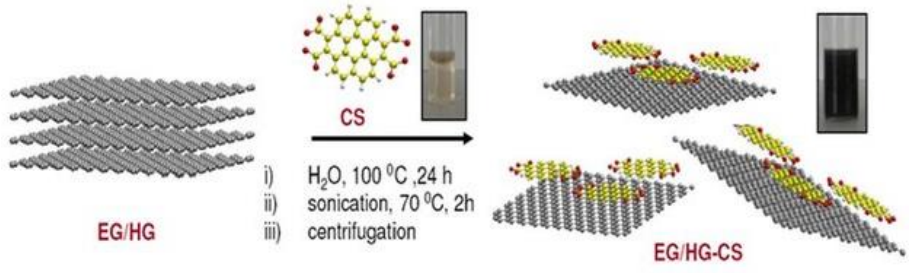

Figure 1.3. Schematic illustration of the thermal (EG) and hydrogen arc evaporation (HG) exfoliation of few-layer graphenes with coronene tetracarboxylic acid (CS) to yield monolayer graphene–CS composites. Reproduced with permission.[110] Copyright 2010, Wiley and Sons.

The biological applications of π–π functionalization of graphene sheets has also been explored and indeed successfully demonstrated (Figure 1.3). Serine protease enzyme chymotrypsin can be immobilized onto GO via this strategy while preserving its native structure and activity.[109] Zhang et al. synthesized a perylene-phosphorylcholine derivative and stacked it onto water dispersible RGO by utilizing π–π stacking. The composite system was shown to be a potentially powerful drug delivery platform for oncological applications.[111]

1.2.1.2 Hydrophobic interactions

The solubility and stability of hydrophobic molecules and nanoparticles in aqueous solutions can often be improved by using amphiphilic copolymers as surfactants. This concept has also been widely applied towards solubilizing or stabilizing hydrophobic graphene sheets under physiological conditions. The formation of RGO/heparin conjugates via hydrophobic interactions has been proven, despite the hydrophilic nature of heparin. RGO is strongly hydrophobic, to the extent that the backbone of unfractioned heparin still would adhere, while the hydrophilic anionic sulfonate groups stabilize the nanoconjugates due to charge repulsion, preventing precipitation and aggregation for 6 months or longer.[112]

Graphene sheets can even be covered with a lipid monolayer due to similar interactions. The hydrophobic lipid tails will adsorb onto graphene, while hydrophilic groups orient themselves towards the aqueous phase (Figure 1.4). The lipid-covered graphene sheets display high stability and are promising candidates as nanocarriers for hydrophobic anticancer drugs.[113] Pluronic is a well-known biocompatible triblock copolymer which can be used to functionalize nanographene oxide (NGO). Pluronic-NGO nanocarriers have been used to effectively deliver methylene blue to tumor cells, leading to efficient and synergistic tumor ablation, both in vitro and in vivo.[114]

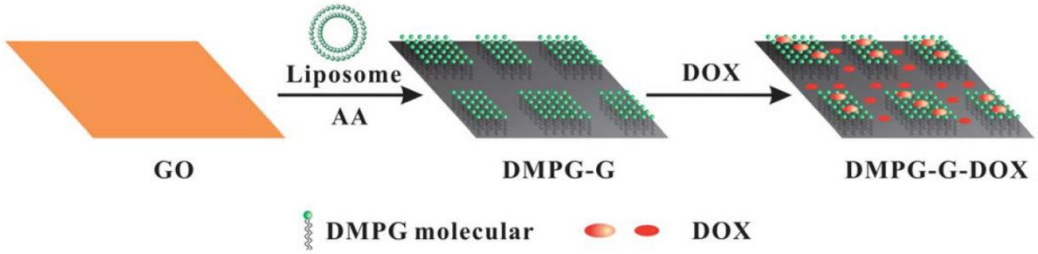

Figure 1.4. Schematic illustration of simultaneous GO reduction via acetic acid (AA) and hydrophobic loading of 1,2-Dimyristoyl-sn-glycero-3-phosphoglycerol (DMPG) liposomes, leading to formation of a lipid monolayer on the graphene sheet. The sheets where then decorated with doxorubicin (DOX). Reproduced from Ref [113] with permission from The Royal Society of Chemistry.

1.2.1.3 Electrostatic interaction

GO exhibits a negative surface charge, due to the oxo-groups introduced during preparation, particularly carboxylic groups. This charge enables non-covalent electrostatic modification of the GO surface with positively charged molecules and polymers. Pristine graphene in theory has no charge, although trace defects still tend to lead to low degrees of charging, depending on the method of synthesis. However, this is typically not appreciable enough for electrostatic conjugation, effectively limiting these techniques to use with GO or with modified graphene sheets. CH/GO complexes, formed from chitosan (CH) and GO, are stabilized by this very type of electrostatic interactions. One advantage of CH and certain other polymers is their compatibility with genipin as a crosslinking agent. Crosslinking CH after adsorption onto GO can produce a bionanocomposite (GCH/GO) that can be cast into a film by a number of conventional techniques. The strongly polycationic nature of CH, along with its biocompatibility, leads to very strong adhesion to GO, yielding homogeneous mixtures with profound potential for biomedical applications.[115] Poly-L-lysine (PLL), another biocompatible positively charged polyelectrolyte, can interact similarly to CH to produce composite GO films or coatings. GO/PLL systems have been widely explored for bio-scaffold applications, particularly as they show positive effects on the proliferation and differentiation of several lines of stem cells.[116]

1.3 Covalent Functionalization

Although graphene is generally thought of as a pristine, continuous layer of aromatic rings, most graphenic materials deviate substantially from this model. GO, the most commonly utilized and produced form of graphene, exhibits many oxygen-containing groups. Carboxyl groups are found primarily along sheet edges or at existing internal defects, while epoxide rings and hydroxyl groups decorate the rest of the sheet. Reduction to RGO can eliminate a large fraction of these groups, but some, especially hydroxyl groups, will always remain. These oxo-functionalities do offer some benefits, for instance they are more reactive than the aromatic rings of a graphene sheet and can be used to covalently modify graphene sheets. Some reactions, namely radical reactions or cycloadditions, can modify not only GO but also pristine graphene, as they occur on defect-free aromatic rings rather than the exposed functional groups.

1.3.1 Modification of Existing Functionalities or Defects

The defect groups found in GO, and sometimes even at very low concentrations in graphene, can be modified by simple organic reactions. Given the regional distributions of these groups, these routes can even lead to regioselective functionalization, although this relies on the regionalized oxidation of GO, rather than systemic control over the post-modification. One significant limitation of defect modification is the need for defects, which can degrade some of the inherent properties of graphene that make it so attractive for these applications. These techniques are generally only relevant for GO or in some cases RGO, rather than more pristine graphene sheets.

1.3.1.1 Carboxylic Groups

Carboxylic groups are known to react easily with amines and hydroxyls. Thus, polymers or other moieties containing these groups can be covalently conjugated to GO, forming amide (Figure 1.5) or ester bonds over the carboxylic functionalities.[117-118] The resulting composite materials combine the properties of GO and the attached molecules, enabling fine tuning of the surface chemistry and other properties.

In recent decades, many natural macromolecules including amino acids, peptides, enzymes, chitosan, and others have been employed to improve certain properties of GO. Many amino acids have been shown to change the interlayer spacing or even the sheet morphology of graphene.[119] Conjugating hydrophilic polymers can tailor the intermolecular interactions of GO derivatives, and is commonly utilized for enhancing aqueous dispersibility. In the case of chitosan-modified GO (GO-CH), 64 wt.% of chitosan was used. GO-CH also shows promise as a nanocarrier for anticancer drugs or genetic material, with a high loading capacity and good dispersibility and biocompatibility.[120] In many cases, it is even possible to maintain high activity of enzymes or drugs conjugated to graphene by adding a polymer spacer.[120-121]

It is generally cheaper and easier to prepare synthetic polymers such as polyethylene glycol (PEG) or polyvinyl alcohol (PVA) than naturally derived macromolecules. Both of these polymers are widely considered to be biocompatible, and thus have been used repeatedly for the surface modification of bionanomaterials. In a paper by Dai et al.,[123] six-armed PEG-amine stars were prepared and conjugated to NGO sheets (<50 nm) via carbodiimide catalyzed amination. The PEG-modified nanographene oxide showed good results as a nanocarrier for SN38, a hydrophobic drug. The behavior of PEG coated nanographene sheets in vivo have been widely studied.[10,73,123-128] In vivo fluorescence

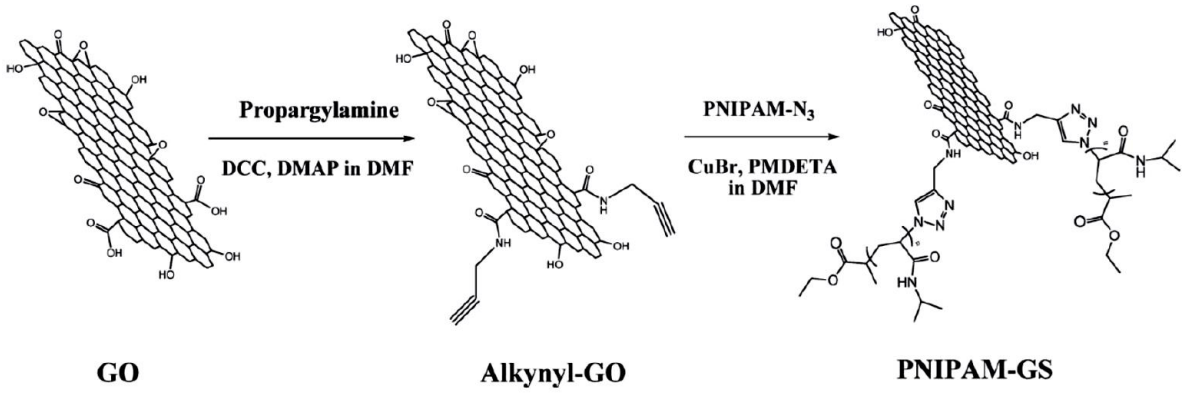

Figure 1.5. Scheme for synthesis of PNIPAM-GO by amide condensation onto GO carboxylic groups. Adapted with permission.[122] Copyright 2011, Wiley and Sons.

imaging has demonstrated the highly efficient passive targeting of nanographene sheets towards tumor cells in several mouse models. Tumor ablation was also observed with a low power near-infrared (NIR) laser, taking advantage of the photothermal properties of graphene sheets.[129] GO can be similarly modified with carbodiimide-activated PVA.[130] Poly(N-isopropyl acrylamide) (PNIPAM) modified nanomaterials are heavily researched due to their temperature-responsive nature. When conjugated to[122] or polymerized from[131] the surface of GO, the resulting nanocomposites combine that temperature sensitivity with the photothermal properties of GO, making them particularly interesting for drug delivery or as smart hydrogels.

1.3.1.2 Modifying epoxy and hydroxy groups

The epoxy groups that decorate the basal plane of GO sheets can also serve as functionalization sites. Nucleophilic ring-opening reactions have been widely reported, often with amine-terminated polymers and a strong base as a catalyst. PLL[132] and 3-aminopropyltriethoxysilane (APTS) (Figure 1.6).[133] for instance have been successfully and homogeneously attached to GO with just such a mechanism. The PLL-GO conjugates exhibited good water solubility and biocompatibility and could have applications as a biomedical nanomaterial. When modified with APTS, the sheets could be easily dispersed in water, DMF, ethanol, DMSO and APTS.

The hydroxyl groups on GO can also be used as the starting point for the functionalization of this nanomaterial and preparation of related derivatives. 2-ureido-4[1H]-pyrimidinone can be reacted with these GO hydroxyl groups thanks to the isocyanates found in the pyrimidinone.[134] It is also possible to first convert hydroxyl groups to form amino[135]

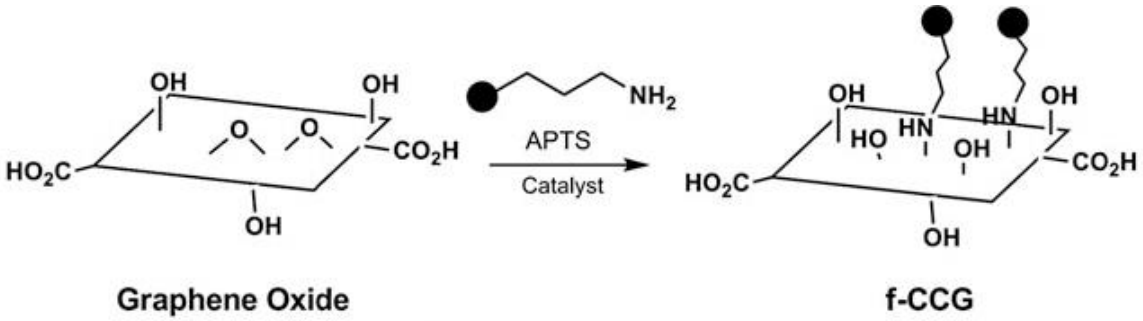

Figure 1.6. Illustration of the reaction between GO and APTS. Adapted from Ref [133] with permission from The Royal Society of Chemistry

carboxyl[136] or thiol[137] groups, which can subsequently undergo a large number of well-documented organic reactions, enabling the preparation of a vast array of GO derivatives.

1.3.2 Cycloaddition Reactions

Cycloaddition reactions are reactions that form cyclic products arising from multiple molecules with unsaturated bonds. Cycloaddition reactions have been heavily utilized for the functionalization of fullerenes and CNTs. Given those successes and the structural and chemical similarities of fullerenes, CNTs, and graphene, it is no surprise that the last decade has seen the further use of cycloaddition reactions with graphene and GO. [24,118,138-144] Three particular cycloaddition reactions comprise the majority of this collective body of work, and all of them are particularly relevant for the synthesis of graphene materials with potential biomedical applications.

1.3.2.1 [2+1] cycloaddition

Nitrene cycloaddition onto graphene has been widely used, owing largely to the relatively broad range of macromolecules containing nitrene precursors or that can be modified to add them. The nitrene [2+1] cycloaddition is also a rather straight-forward reaction that will proceed under most reaction conditions. Carbenes – nitrene analogues where a carbon atom has a lone electron pair, instead of a nitrogen atom – can also react with graphene. Both will bond across two adjacent carbon atoms from graphene, forming aziridines or cyclopropanes, respectively. Both variants of [2+1] cycloaddition are similar to the Bingel reaction, although the Bingel reaction proceeds under its own distinct mechanism, relying on different reactants. All three reactions are non-regiospecific, producing homogeneously functionalized graphene derivatives. This is relatively unique, as many methods for the covalent functionalization of graphene display at least some specificity.

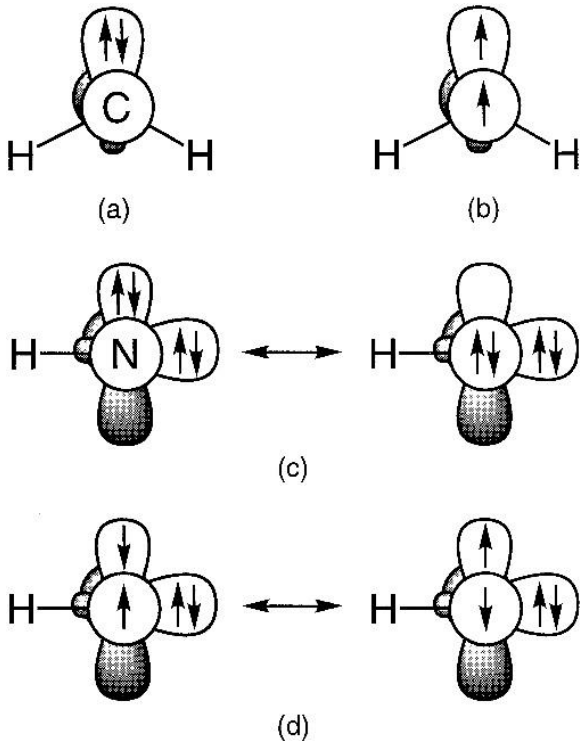

Figure 1.7. Schematic depictions of the lowest a) singlet and b) triplet states of methylene and of c) "closed-shell" and d) "open-shell" components of the lowest singlet state ($^1\Delta$) of nitrene. Reproduced with permission from [147] Copyright 2000 American Chemical Society.

The mechanism of reaction for nitrene and carbene [2+1] cycloadditions is analogous, so only that of carbenes will be explained in detail[145] Carbenes are sp^2 carbons with a free electron pair that is found in either a triplet state – split between the free sp^2 and p orbitals – or in the singlet state, where both are in the sp^2 orbital (Figure 1.7). Detailed characterization demonstrates that carbenes can be found with bond angles of either 130-150 $^\circ$ or 100-110 $^\circ$, arising from triplet and singlet carbenes, respectively. [145-146]

Carbene cycloaddition can be stereoselective when conjugating to stereoisomeric alkenes, if the carbene used in the reaction is primarily found in a singlet form. This difference arises due to the stepwise reaction of the lone electrons if they are split across two orbitals, as in the triplet state. Singlet carbenes react in a concerted step, removing the opportunity for the newly forming stereocenter to transition between the first and second step of the triplet reaction (Figure 1.8). Stereospecificity is, however, a non-factor with graphene. Even with doped or defective hexagonal lattices, the low density of such stereoisomer sites in graphene materials makes the chances of a cycloaddition occurring at such a site negligible when compared to the total surface of these materials.

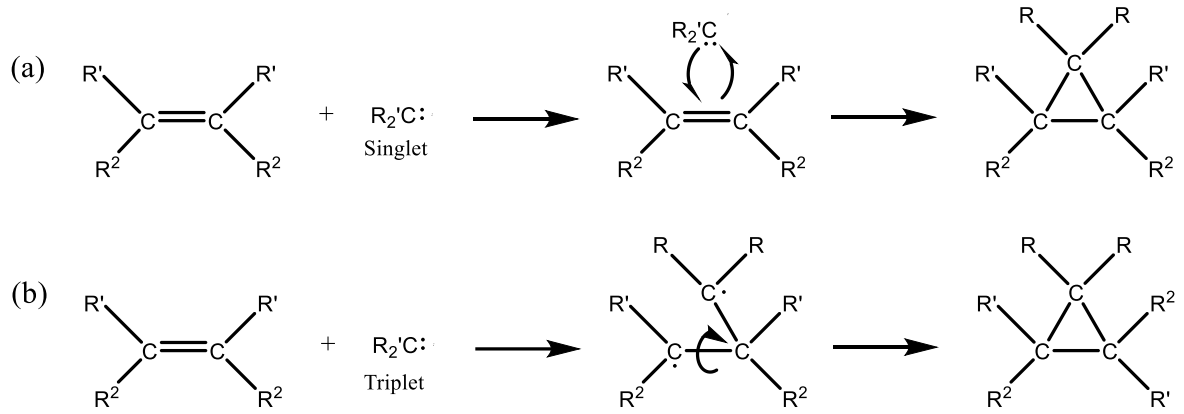

Figure 1.8. Schematic reactions of a) singlet and b) triplet carbene with alkenes. In reaction b), note the broken alkene bond is free to rotate, resulting in a loss of stereoselectivity.

Carbene cycloaddition reactions are quite robust, tolerating but not requiring aqueous or polar solvents.[148] The reactions can proceed with GO, RGO, or pristine graphene materials, [149] and the degree of functionalization can often be tuned simply by controlling the reaction temperature and initial ratios of graphenic material and carbene.

Nitrene cycloaddition has been more widely explored than carbenes, owing largely to the relative ease of synthesizing azide-containing molecules. Azide groups can form nitrenes in-situ via heating, allowing for more stable reactants than carbenes, and a more controllable reaction.[25,150]

Carbene cycloaddition onto carbon nanomaterials began in the 1990s with fullerenes[150-151] before next being demonstrated with CNTs.[47,152] Applications with graphene were explored only much later, in an attempt to adjust the electronic properties of graphene sheets and tune their band gap. This effect was successfully demonstrated with dichlorocarbene,[153] where the lowest unoccupied molecular orbital (LUMO) band of dichlorocarbene and the highest occupied molecular orbital (HOMO) band of the conjugated graphene bonds can interact, followed by the HOMO electron pair from carbene interacting with the empty π^* antibonding orbital of graphene.[118]

Research interest in carbene cycloaddition onto graphenic materials has been limited, especially compared to the significantly broader past efforts with both fullerenes and carbon nanotubes. More recent investigation has been limited to computational modelling[154] and brief mentions in review articles.[48,63,118,155-156] Dibromocarbene was shown to tune the band gap of graphene nanosheets (Figure 1.9) which may indicate that carbene cycloaddition does not negatively impact the sp^2 hybridization of graphene under certain conditions.[157] It is possible that this electronic tuning with carbenes could reignite interest.

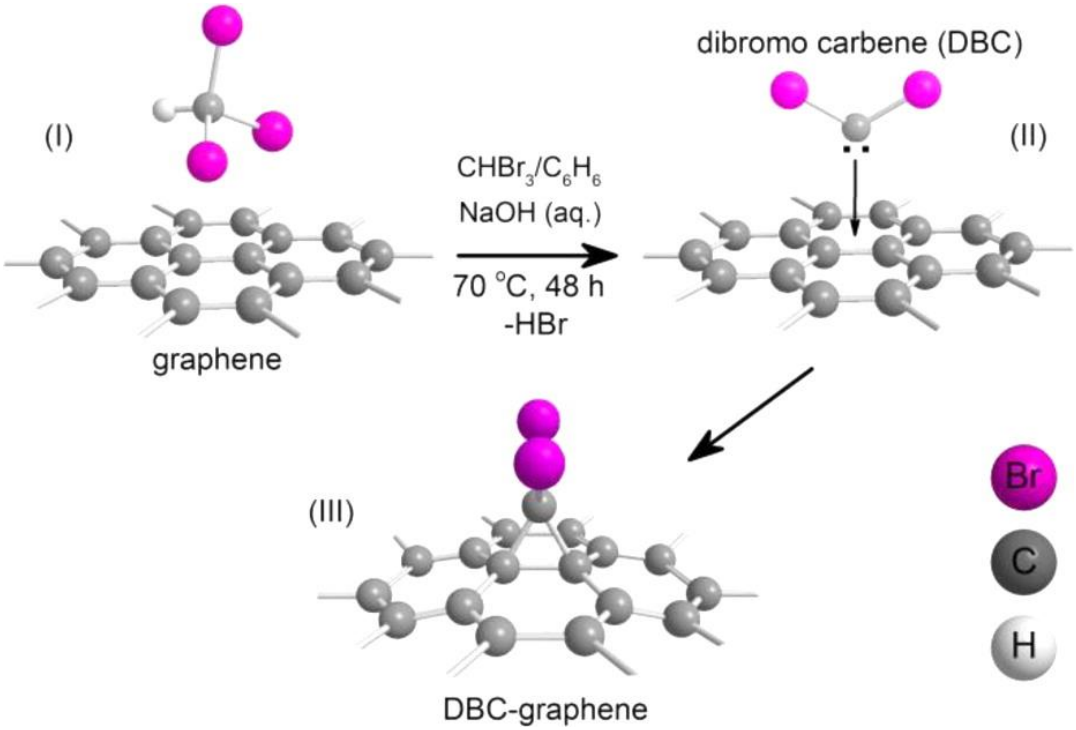

Figure 1.9. Dibromocarbene (DBC) functionalization of graphene via the formation of dibromocyclopropyl adducts tangential to the lattice plane. Reproduced with permission from [157] Copyright 2016 American Chemical Society.

Research into nitrene cycloadditions follows a similar historical trend, having grown rapidly since 1994, first with fullerenes, then carbon nanotubes, and finally with graphene. Unlike most carbene precursors such as diazo compounds, nitrene precursors – typically azides – are comparatively stable, and can be stored and handled more easily, while activation can be achieved still under relatively mild conditions.[158-159] Given the broad portfolio of organic azides that can be purchased commercially or prepared in the lab, their widespread utilization for functionalization of graphene is easy to understand.

The triazine-based azide derivative developed by our research group and used extensively in this work, 2,4-dichloro-6-azido-1,3,5-triazine (Trz), has been shown to not only maintain the sp^2 network of graphene even after conjugation, but even to integrate into the electronic system, forming a hybrid material.[28,51,160] Indeed, our group recently reported the use of it to simultaneously functionalize and *p*-dope nanographene.[106] Instead of forming an aziridine ring as generally expected with [2+1] nitrene cycloaddition, the graphene substrate underwent re-hybridization, producing an open [4,4,1] bicyclic structure (Figure 1.10a). The major consequence of this is the interaction of the lone electron pair from the bridging nitrogen atom seemingly interacting with the electronic system of the nanographene

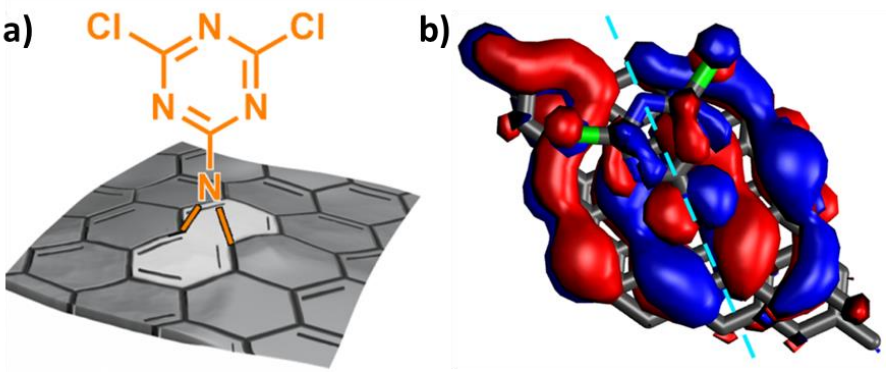

Figure 1.10. a) Structure and b) HOMO electron distribution of Trz after conjugation to graphene. Modified with permission.[106] Copyright 2019, Wiley and Sons.

as a *p*-type dopant (Figure 1.10b). The chlorine functionalities of the triazine group also enable post-modification in a stepwise and controlled manner. Their reactivities are sufficiently different that they can be replaced in sequential reactions via careful temperature control, it is possible to attach two unique molecules to each triazine, or to increase functionalization density of a singular substituent.[149]

Nitrene cycloaddition is a widely applied and extremely versatile technique for the covalent modification of carbon nanomaterials. In particular, the implications of electronically integrated functionalities being covalently added to graphene or graphene oxide could have major benefits for all applications where electronic properties are important. As a result, nitrene cycloaddition has seen rapid growth in electronic and biological applications, including the preparation of novel battery or supercapacitor materials,[161-162] antibacterial platforms,[163] and printable bio-ink,[88] amongst others.

1.3.2.2 [3+2] cycloaddition

1,3-dipoles act in a [3+2] cycloaddition almost like a diene where the four *p* electrons are shared across three atoms. Most of the commonly used 1,3-dipoles consist of oximes or nitrones, or other species where nitrogen is bonded to one or more oxygen atoms. These dipoles can react with alkenes in a concerted cycloaddition reaction, not dissimilar from a [4+2] Diels-Alder (DA) cyclization. In a [3+2] cycloaddition, the diene and dienophile are replaced instead with a dipole and dipolarophile. One noticeable difference with a [3+2] cycloaddition is that simple and electron-deficient alkenes can still function as dipolarophiles, as dipoles are both electro- and nucleophilic. Depending on the dipolarophile, the dipole can react over the LUMO or the HOMO band. In the case of graphene as a dipolarophile, the 1,3-dipole will serve as the HOMO, while the dipolarophilic centers on graphene act as the LUMO (Figure 1.11).

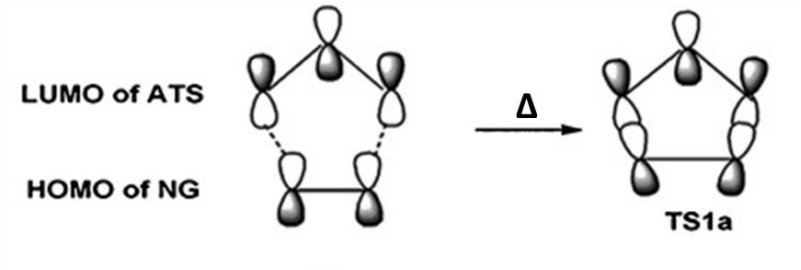

Figure 1.11. Orbital interactions of azidotrimethyl silane (ATS) and nanographene (NG) in a [3+2] cycloaddition reaction. Adapted with permission.[164] Copyright 2012, Wiley and Sons.

[3+2] cycloadditions, as with the other cycloadditions, were first demonstrated with fullerenes[138,165-166] and then CNTs[167] before being applied with graphene and GO.[141] Most [3+2] cycloadditions onto graphene or GO have centered around the use of a narrow range of 1,3-dipoles such as azomethine ylides,[48,141,168-169] pyridinium ylide[170] or azidotrimethylsilane[164,171] Molecular simulations indicate that carbonyl ylides could also react readily with graphene, although they have not yet been widely adopted or explored experimentally.[172-173] Azomethine ylide cycloaddition (Figure 1.12) has generated significant interest, especially due in part to the lack of regiospecificity of [3+2] cycloadditions onto graphene.[174] Azomethine ylides can conjugate throughout the surface of graphene sheets, with comparatively good homogeneity. Other functionalization reactions occur predominantly in specific regions of graphenic materials, for instance amide conjugation onto the carboxylic groups present in graphene oxide primarily functionalizing the edges of sheets, as would be expected based on the distribution of oxidized moieties on GO.[71-72]

Some azomethine ylides can be stable enough to be synthesized independently and handled or stored, but they are typically produced in situ starting from one of many single- or multi-component precursors. The most relevant route for graphene functionalization is condensation of aldehydes and amines or carbonyls with sarcosine. Other methods to produce azomethine ylides include aziridine ring opening or deprotonation of imines and iminiums. Azomethine ylides prepared from aziridines are typically stereoselective, as they will react with most dipolarophiles faster than the substituent groups can rearrange. However, given that stereoisomerism is typically less of a concern for graphene modification, the ease and flexibility of aldehyde-ketone condensation has made it the most common starting point for [3+2] cycloadditions onto graphene.

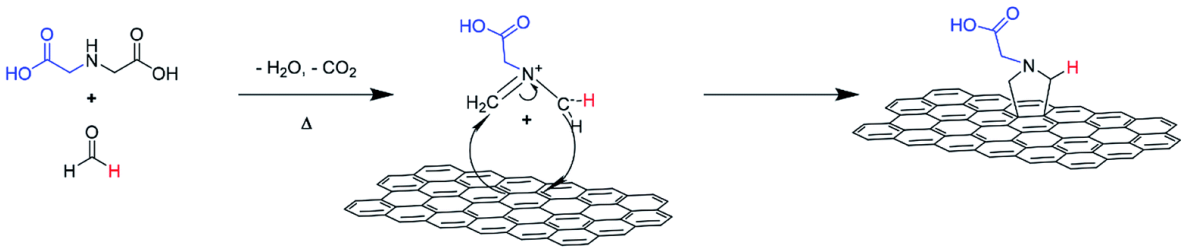

Figure 1.12. Scheme of 1,3-dipole formation and subsequent [3+2] cycloaddition for azomethine ylides and graphene.[83] Published by The Royal Society of Chemistry.

While these cycloaddition reactions are homogeneous across the surface and edges of graphene sheets, the effects of the functional groups on the neighboring graphene atoms is dependent on the position of the functional group relative to the graphene sheet. When conjugated to the edges of a sheet, these 1,3-dipoles can form 5-membered rings while distorting only the specific rings of graphene to which they bond, as the hexagonal rings at the edge of a sheet are less constrained by neighboring rings. In contrast, functionalities on the central regions of the sheet will distort multiple rings due to the tension introduced by the bond length differentials. This can also disrupt the conjugated π-system of graphene, which would negatively impact many electronic properties. The breadth and ease of synthesis of 1,3-dipoles, especially substituted azomethine ylides, make them extremely interesting and useful despite the drawbacks that can arise such as impaired electronic properties. [3+2] cycloadditions are a uniquely simple and versatile method for functionalizing graphene or GO.

Despite the frequency with which [3+2] cycloaddition reactions are still used and reported in literature, there has been only minor development or improvement to such reactions as compared to other cycloaddition routes. Recent improvements have been limited mostly to the attachment of increasingly complex moieties, still centered mostly around azomethine ylides, as well as the optimization of solvent-free reaction conditions for some systems.[83] Perhaps the most interesting demonstration of a [3+2] cycloaddition reaction does not involve the functionalization of graphene materials, but rather the bottom-up synthesis of N-doped nanographene from 3-phenyl-pthalazinium-1-olate via mild heating in ambient atmosphere.[175] Here, a fully synthetic graphenic material with 10% intrinsic nitrogen doping was produced with no additional reagents or solvents. While this is not, strictly speaking, a [3+2] cycloaddition functionalization reaction, the ability to produce graphene bottom-up via wet chemistry, doped or otherwise, is certainly noteworthy. There

are several intriguing applications for such doped nanographenes, especially for metal-free catalysis, as well as for nanoelectronics and high-temperature coatings.

1.3.2.3 [4+2] cycloaddition

Diels-Alder (DA) reactions are perhaps the most famous cycloaddition reaction. As with [3+2] cycloadditions, they involve six electrons acting in concerted movement, with a diene and dienophile that combine to form a six-membered ring. The DA reaction has been very thoroughly investigated, and the mechanisms and outcomes have been well-described.[45,144,176-186] It is highly stereoselective, and this selectivity is a point of emphasis for organic synthesis via DA cycloaddition. There are still no reported examples of beneficial stereoselectivity of DA products using graphene, due partially to the emphasis on conjugating polymers or macromolecules. These large functionalities extend far beyond the surface of the graphene, rendering any interactions at the chiral center adjacent to the sheets relatively inconsequential. Even when smaller molecules are conjugated, the chiral center is comparatively inaccessible due to the steric effects of having an extremely large graphene sheet in direct contact with the chiral carbon center.

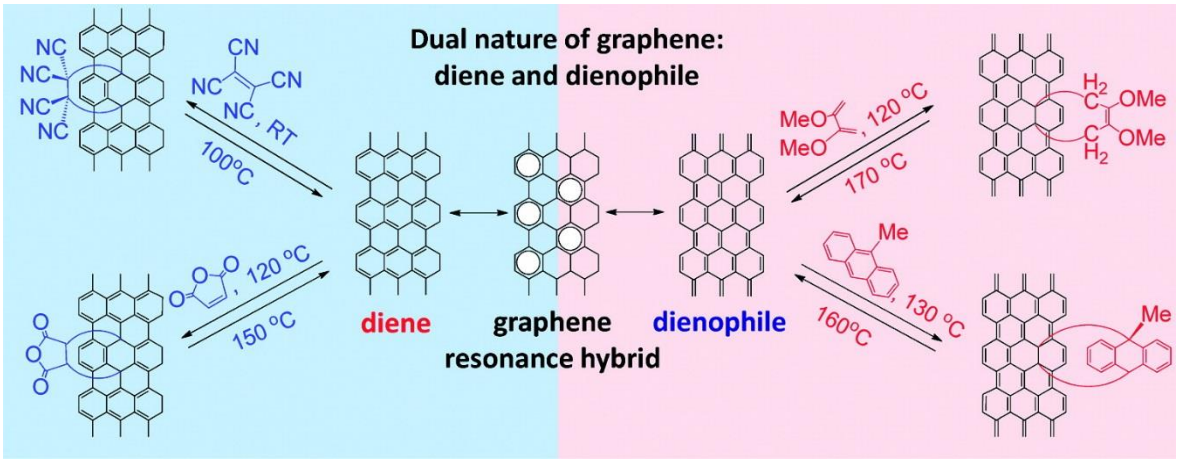

Figure 1.13. Examples of several [4+2] cycloadditions with graphene acting as diene (left, in blue) and dienophile (right, in pink). Adapted with permission.[178] Copyright 2012, American Chemical Society.

Graphene is unique when it comes to DA reactions, as it can play both roles in the reaction. With its repeating, tessellated sp^2 rings, graphene can act as either a diene or a dienophile (Figure 1.13).[176] Furthermore, multiple theoretical assessments have provided

strong evidence that DA reactions with graphene are very regioselective.[144,181] Even when accounting for defects, [4+2] cycloadditions onto the basal plane of graphene sheets seem to be much less likely than closer to the edges of the sheets, due to the significantly higher energy of the products as compared to the reactants. In both the diene and dienophile role, single-vacancy defects in graphene would be expected to significantly reduce the energetic barriers for conjugation, suggesting that such defects would enhance or increase the functionalization of the basal plane via DA reactions.[144] The edges of graphene sheets would still be the most likely reaction site for any DA reaction, especially along unsaturated armchair edges, where both diene and dienophile regions can be readily and favorably expressed.

Experimental results do partially support these predictions, with certain DA reactions being regioselective to the edges of graphene sheets,[182] while some appear broadly homogeneous.[183,187] The outcome seems to be strongly influenced by the precise reaction conditions and methods, as mechanochemically driven reactions with maleic anhydrides appear edge-specific,[182] while the same dienophile was homogeneously conjugated under multiple conventional solution reactions.[45,144,183] Detailed exploration of regiospecific reactions has been rather piece-meal, with many papers not fully investigating such aspects of their products, showing only that conjugation was successful, without characterizing further the positional distribution of functional groups. Some in literature have even criticized this minimal level of characterization, pointing out that many papers do not conclusively show that conjugation truly occurred via a DA mechanism[183] While it is clear that armchair edges of graphene sheets will react more readily via [4+2] cycloadditions than the basal plane of the sheets, both are not only possible but demonstrable occurrences.

Conjugation of maleic anhydride as a dienophile to graphene as a diene has been the most widely implemented DA cycloaddition for graphenic materials.[176,188] Tetracyanoethylene has also been widely used, and was even investigated as a method to produce graphene from graphite via conjugation and exfoliation, followed by a reverse DA to restore the pristine sheet structure to the graphene layers.[187] Other dienophiles such as maleimides[182] – imide analogues to maleic anhydrides – or benzyne[189] have also been conjugated to graphenic materials via DA reactions of dienes on graphene materials, but not with the frequency or level of detail seen with maleic anhydride. Maleimide derivatives with N-(1-oxyl-2,2,6,6,-tetramethyl-4-piperidinyl)-maleimide (TEMPO-MI) catalysts or N-(2,2,6,6,-tetramethyl-4-piperidinyl)-maleimide (TEMP-MI) precursors have also been conjugated to graphene in a one-pot, simultaneous exfoliation and functionalization

process.[188] Previous reactions with maleimides were multi-step processes where graphene or graphene oxide was prepared in a separate process. These nitroxyl-modifed graphene sheets show higher charge capacity, making them very promising for redox applications such as energy storage, or for use as an electrode material. Furthermore, the presence of catalysts on the surface can enable in situ polymerization to produce graphene-polymer nanoconjugates.

Graphene has been used as a dienophile with only a small number of dienes, namely cyclopentadiene derivatives.[179-180] It is easy to see why these dienes have become a focal point, as it is comparatively easy to synthesize a wide range of polymers and macromolecules with cyclopentadienyl groups. The subsequent DA conjugations are also robust and straight-forward. The combination of both benefits makes cyclopentadienes one of the more useful functionalization routes for DA reactions with graphene.

Furan derivatives have also emerged, led by furfurylamine, for indirect two-step DA functionalization of graphene oxide.[185-186,190] The furans can grafted onto the carboxylic groups present in graphene oxide, and can be subsequently post-modified through DA reactions. While these are only indirect cycloadditions where the graphene sheets are not directly involved, it is worth highlighting self-healing or shape memory properties that arise in such nanocomposites, as the furfuryl groups readily undergo repeated DA and reverse DA reactions.[45,190] Furthermore, the presence of graphene, with its photothermal properties, allows for easy localized warming of such materials under NIR irradiation, an appealing trait for any self-healing systems, whereby damaged regions of the composite can be irradiated to promote and accelerate re-conjugation.[190]

DA reactions form an important pillar of graphene and graphene oxide functionalization. It is possible to conjugate both dienes or dienophiles to graphenic materials, and through selection of reagents and reaction conditions, regiospecific control can even be exerted.[176,178,182] The robust and simple nature of these reactions, along with the lack of byproducts, makes them very interesting for a range of applications, for instance producing biomedical nanomaterials, where toxicity of reagents or byproducts can be of great concern.[63,118] Further, DA reactions have shown the capability to carefully and controllably tune electronic properties of graphene,[180] opening the doors for a wide range of optoelectronic applications.

1.3.3 Radical reactions

Free radical reactions can covalently modify graphene (Figure 1.14). Polystyrene can be grafted onto RGO sheets via diazonium addition and atom transfer radical polymerization (ATRP) reactions, yielding composites with polymer content as high as 82 wt%. The Young's modulus and tensile strength of these nanocomposites increased by 57.2% and 69.5% respectively, as compared with a pristine polystyrene film.[191]

Self-initiated photografting and photopolymerization (SIPGP) has been demonstrated as a method to grow polymers from graphene sheets without requiring an initiator. Ultraviolet (UV) irradiation of the graphene sheet graphene abstracts hydrogens at defects where sp^3 carbons can be found, leading to the formation of free radicals. The formed carbon radicals can then initiate radical polymerization of vinyl monomers, producing polymer brushes with homogeneous coverage of the graphene sheet. Under optimized conditions, relatively narrow PDI can even be achieved. Sharp et al. directly modified graphene sheets with styrene using SIPGP. CVD graphene, epitaxial graphene on SiC, and RGO were all modified to confirm the broad utility of this technique (Figure 1.15).[192]

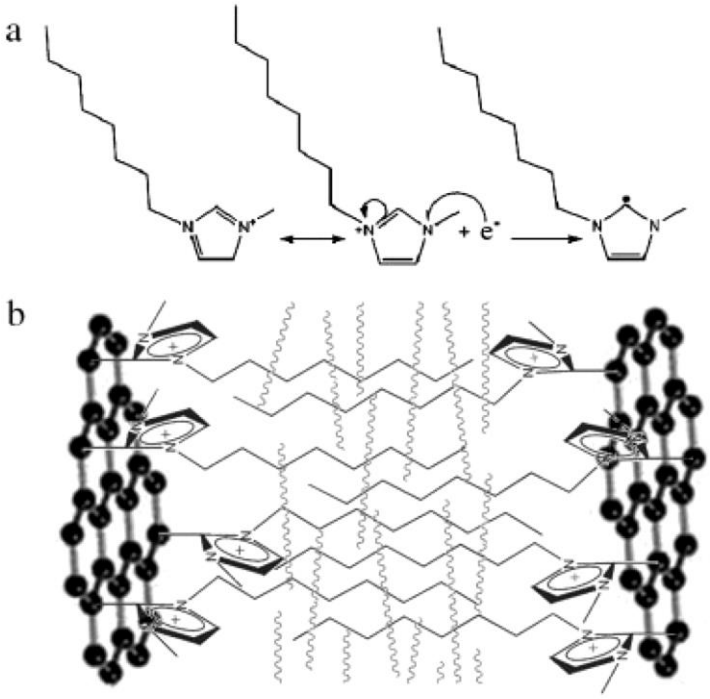

Figure 1.14. Scheme of a) 1-octyl-3-methylimidazolium radical formation and b) Attraction of GNSILs to similar groups in the polymer. Reproduced with permission.[193] Copyright 2008, Wiley and Sons.

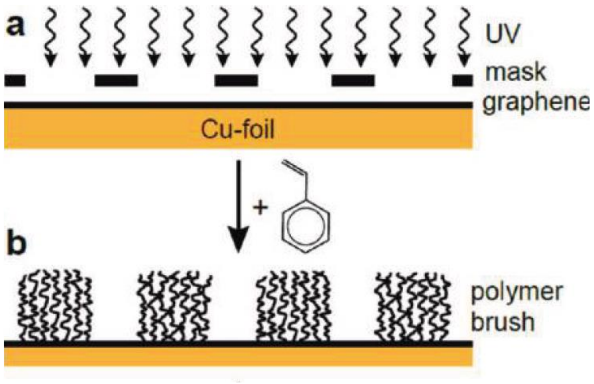

Figure 1.15. Patterned polymer brush layers on CVD-grown single layer graphene are prepared by UV illumination through a mask in bulk styrene. SIPGP occurs selectively in illuminated regions of the material. Adapted with permission.[192] Copyright 2011, American Chemical Society.

Graphene sheets functionalized via SIPGP with N,N-dimethylaminoethyl methacrylate (DMAEMA) were successfully applied as biosensors to detect the neurotransmitter acetylcholine based on the transduction of pH sensitive groups.[194] Complex graphene-polymer conjugates can be prepared using SIPGP, especially when synergistically combined with other techniques. SIPGP grafting of polystyrene (PS) or PDMAEMA has been combined with GO-CH composites where chitosan was attached to only one side, leading to the formation of Janus particles. By varying both the vinyl monomers used and the irradiation time, the brush length and properties can be controlled and tuned with remarkable precision.[195]

1.4 Fluorous Biphasic Systems

Catalysts are often very expensive and very toxic. Furthermore, many catalysts are not rendered inactive over the course of a reaction. [196] Therefore, the ability to capture, purify, and reuse a catalyst is a major point of emphasis for green chemistry on industrial scales. One well-known method to achieve this is fluorous biphasic catalysis.[196-203] For practical reasons, catalyst recycling only makes sense if it is relatively simple and affordable to collect a large fraction of the used catalyst with techniques such as chromatographic separation or filtration, to name a few, without negatively impacting the activity and efficiency of the catalyst.[204-205]

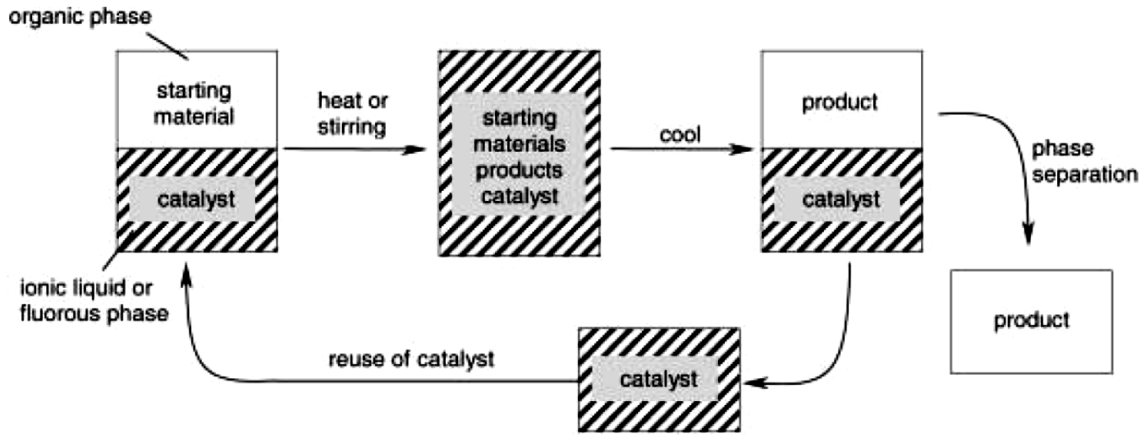

Figure 1.16. Principle of a simple work-up procedure when using fluorous-phase chemistry or ionic liquids. Reproduced with permission.[201] Copyright 2002, Wiley and Sons.

Fluorous biphasic systems come into play due to the unique properties and interactions of highly fluorinated molecules. For one, they are typically immiscible with both aqueous and organic solutions, owing to the combined hydrophobic and lipophobic nature of fluorinated compounds.[198] Due to strong fluorous-fluorous attractions, fluorinated compounds also display a high affinity for each other.[199] Thanks to the combination of strong cohesive forces and poor interactions with most other solvents, fluorous phases tend to form and separate from aqueous or organic phases under standard conditions.[197-199] However, the separation of the fluorous phase has been shown to be temperature-sensitive, generally becoming miscible upon heating (Figure 1.16).[197,199]

This temperature-regulated separation is the crux of fluorous biphasic catalysis, whereby a fluorinated catalyst can be controllably homogenized during a reaction, and then separated with high partition coefficient after cessation and cooling of the reaction mixture.

This principle was first demonstrated by Horváth and Rábai, who modified triphenyl phosphine with perfluorinated chains, and added a fluorous solvent in addition to a hydrocarbon phase.[197] Since then, the concept has been developed extensively, with an ever-growing catalog of fluorinated catalysts[197,201,203-204] emerging. Moreover, solid-state alternatives to fluorous solvents have arisen, partially addressing the challenges facing these systems.[206-208] Fluorous solids form a solid-liquid biphasic system, whereby separation of the fluorous phase can be achieved more easily as compared to a liquid-liquid system.[206-209]Most of these solid-state fluorinated scaffolds are designed with column chromatography in mind for phase separation, for instance with perfluoroalkylated silica gels.[201,206-210] The strong fluorous interactions between the catalyst or reagent and these surface-modified silica

beads lead to longer retention times, allowing effective separation from the non-fluorinated reagents and solvents with relatively high purity and efficiency.[203,211] Such solid-state supports are still far from ideal, however, as chromatographic separation faces limitations in terms of speed – the faster a column is run, the more difficult it is to separate the phases – and throughput capacity.[203,205,212] Fluorous polymers such as Teflon have also been used as solid-state systems, with reasonable success. However, such systems often require higher temperatures to homogenize catalysts, and some catalyst is often trapped within the fluorous polymer and cannot be effectively released and activated.[209]

2 Scientific Goal

Graphene and GO have rapidly become two of the most exciting and intensively explored materials for applications ranging from electronics to biomedicine.[79,102,213-216] The realization of the promise and potential of graphenic materials faces a number of hurdles. The first major challenge to overcome is the development of methods for mass production of high quality graphene sheets.[79,216-217] Currently, there is a tradeoff whereby CVD methods can produce near-pristine graphene, but only in very limited quantity.[6,64,218-219] Meanwhile, Hummer's method and its variations can be run at industrial scales, but the produced GO is inferior to graphene in many regards – especially in its electronic properties. This barrier is further amplified with nanographene, where lateral size is below one hundred nanometers.[69] Such nanosheets are, however, particularly useful for a number of fields. This size range would offer unique benefits for biological applications like drug delivery, where the enhanced permeation and retention (EPR) effect would improve drug targeting for tumors.[8,123-124]

As a result, the first goal of this thesis was to develop a new method for the scalable production of nanographene sheets of high quality and with a narrow range of sizes. Given the limitations of scale with existing methods for graphene production, including CVD and liquid phase exfoliation techniques, along with the defect concentration that arises through current large-scale methods centered around oxidation and exfoliation, this required a new approach to graphene synthesis (Figure 2.1).

There is very limited literature showing the ability of sodium hypochlorite to degrade CNTs and graphenic materials,[38,55,98] although the actual mechanisms of the interaction are poorly elucidated. One hint was the formation of graphene quantum dots when larger graphene sheets were exposed to hypochlorite. We hypothesized that the most likely mechanism, given the lack of chlorination of these quantum dots, was some sort of cutting reaction whereby hypochlorite opens bonds in the graphene planes, and at a certain critical degree of reaction, smaller fragments may be cut and freed from the larger sheet.

Figure 2.1. Scheme for mild, scalable nanographene synthesis**.** Sodium hypochlorite acts as a mild oxidizing agent to activate the graphite flakes. Subsequent ultrasonication exfoliates nanographene sheets from the bulk graphite material.

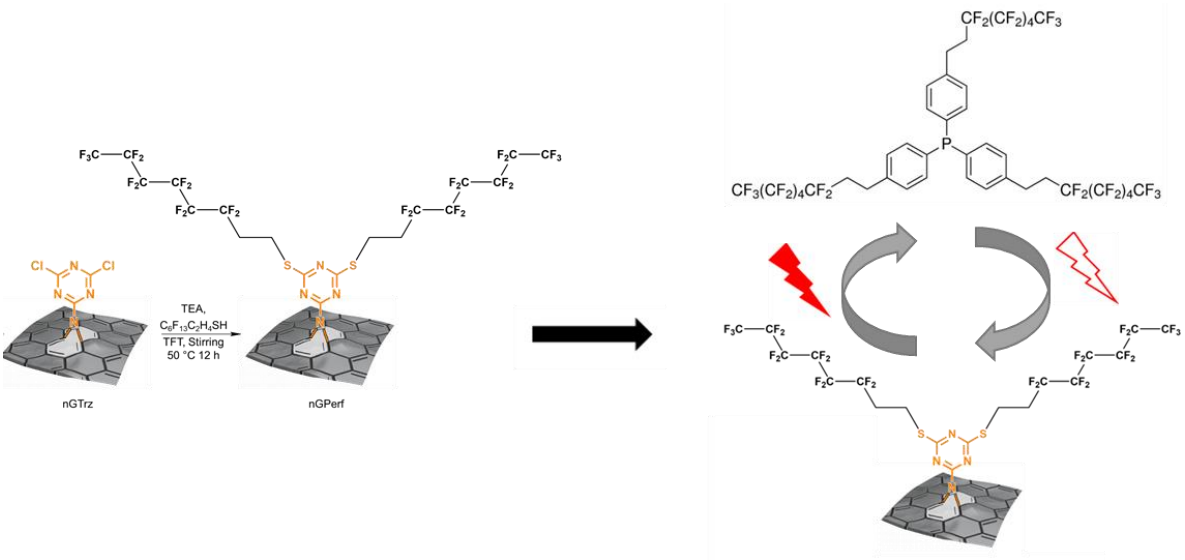

Figure 2.2. Conceptual plan for nGTrz perfluoroalkylation, and subsequent photothermally triggered fluorous biphasic catalysis.

Based on our interpretation of these studies, we will investigate an approach using very dilute hypochlorite solutions and starting directly from graphite. The goal is to directly cut graphene nanosheets out of the graphite particles, with no or minimal introduction of oxygen containing groups and other sp^3 defects that would disrupt the intrinsic properties of the nanographene (nG). As no known reaction mechanisms, conditions, or kinetics had been reported for such a process, we need to start from the beginning, testing a broad range of parameters and investigating the results.

In order to fully utilize and take advantage of the benefits of the new nanographene synthesis developed in the first stage of this project it is necessary to functionalize them. Using a method developed previously in our research group, Trz will be conjugated via a [2+1] nitrene cycloaddition mechanism.[28,51,149] This will lead to the second goal of this thesis – an in-depth characterization of the nG and modified nGTrz sheets. The structural and chemical properties, as well as spectroscopic and electronic properties, will be probed to shed light on the unique interactions between the nG plane and the conjugated Trz groups. Previous work with CNTs and Trz had suggested that the nanocomposites could be prepared with little or no degradation in the π-conjugation of the CNTs, and accordingly their electrooptical properties, despite high degrees of functionalization.[51]

The two chlorines on each Trz group offer versatile functionalities for post-modification, and nGTrz provides a unique 2D multivalent platform upon which to build. With the increasing focus on green chemistry, techniques for recycling or separating costly or toxic compounds such as catalysts is of growing importance.[210] Fluorous biphasic systems leverage the temperature-dependent miscibility or solubility of fluorinated materials with organic or

aqueous solutions to reversibly mix or separate specific molecules from a reaction mixture. This can be applied with fluorinated catalysts or reagents, in order to recycle or purify them after a reaction.[202,210,220-221] Such biphasic systems have been widely used in academic work, but the transition to industrial application has remained elusive due to a number of challenges. Firstly, many systems rely on the use of fluorous solvents, which are often expensive, toxic, and costly to handle or dispose of.[205,209,220] Secondly, the separation and recycling of fluorous catalysts can often be a complex and time-consuming process.[210]

The final goal of this project is the development of applied derivatives of nGTrz to address these limitations and present a practical and beneficial solution for biphasic systems. To achieve this, nGTrz will be modified with perfluoroalkanes (PF) in order to produce a solid-state fluorous platform (nGTrz-PF), which is then loaded with fluorinated phosphine catalyst (fTPP). The loading will be carefully characterized and then tested subsequently with NIR-triggered release based on the photothermal effect of the nG sheets in the nanosystem. Upon successful repeated release and recapture of catalyst, the utility of nGTrz-PF and fTPP will be demonstrated with the Appel chlorination of two different alcohols.

3 Publications and Manuscripts

3.1 Scalable Production of Nanographene and Doping via Nondestructive Covalent Functionalization

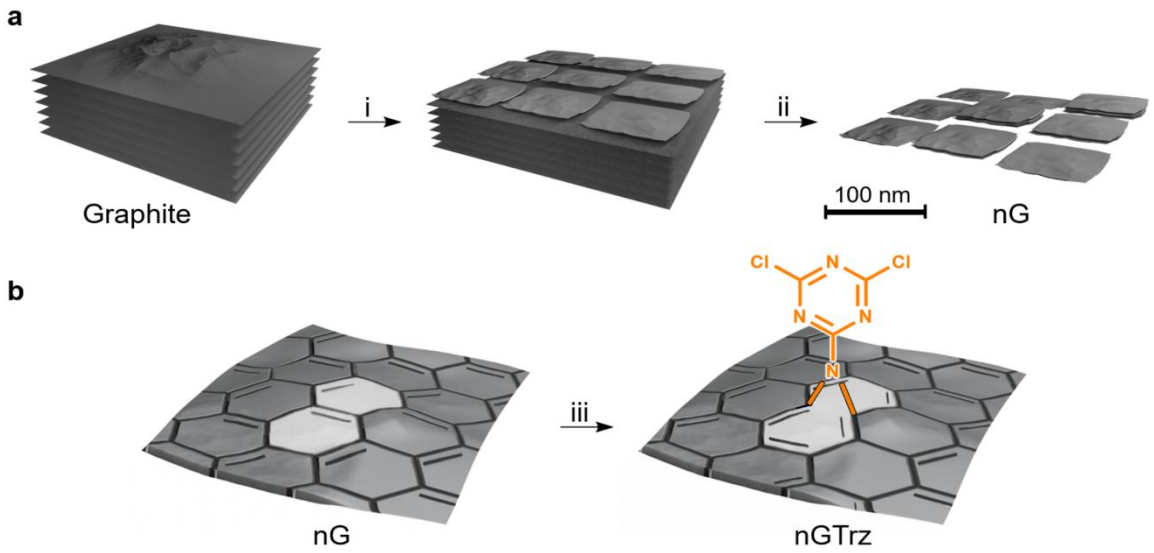

Figure 3.1. Schematic representation of a) nG production and b) functionalization. The carbon atoms in the cycloaddition reaction site are sp^2 hybridized after functionalization, maintaining the aromaticity of the system. Reproduced with permission.[106] Copyright 2019, Wiley and Sons.

Guy Guday, Ievgen S. Donskyi, Mohammad Fardin Gholami, Gerardo Algara-Siller, Felix Witte, Andreas Lippitz, Wolfgang E. S. Unger, Beate Paulus*, Jürgen P. Rabe*, Mohsen Adeli*, and Rainer Haag*

Small **2019**, 1805430. https://doi.org/10.1002/smll.201805430

Author Contribution

Guy Guday and Ievgen Donskyi conceived and designed this project, synthesized all nG and nGTrz compounds, and prepared the manuscript. Guy Guday performed Raman, SFM-TM, and FTIR experiments. Ievgen Donskyi, Andreas Lippitz, and Wolfgang Unger performed and analyzed XPS and NEXAFS experiments. Mohammad Fardin Gholami and Jürgen Rabe performed SFM-PFTUNA experiments. Gerardo Algara-Siller recorded all HR-TEM results, and Felix Witte and Beate Paulus performed all simulation studies. Mohsen Adeli and Rainer Haag provided scientific guidance and suggestions and corrected the manuscript at all stages.

3.2 Reversible photothermal homogenization for fluorous biphasic systems with perfluoroalkylated nanographene

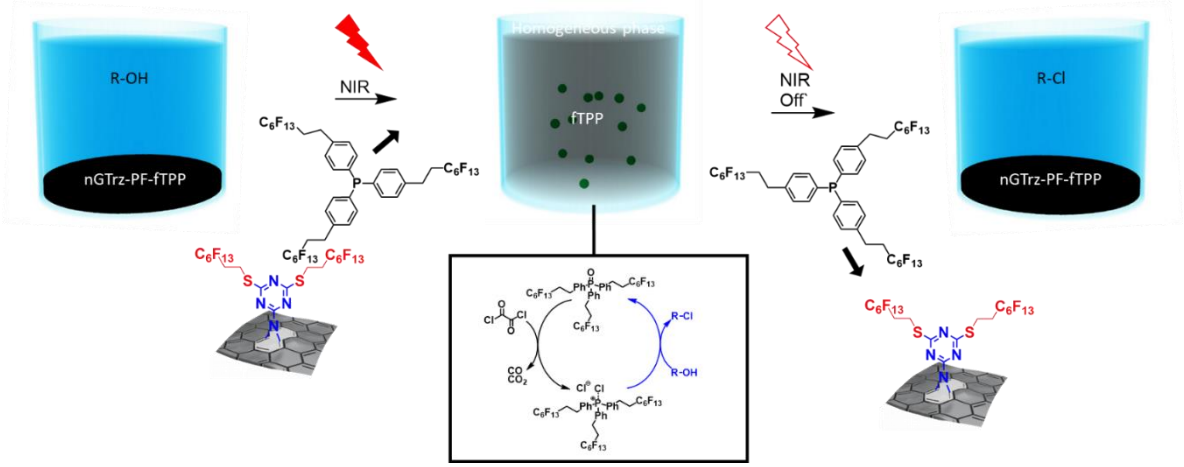

Figure 3.2. a) Scheme of catalyst release and homogenization in the nGTrz-PF solid-liquid biphasic system. Upon irradiation, fTPP catalyst is released and the system is homogenized through photothermal heating of nG. When irradiation is ceased, the fluorous phase aggregates upon cooling. Detailed views of b) catalyst regeneration and c) Appel chlorination are shown in the callouts.

Guy Guday, Philip Nickl, Mohsen Adeli*, and Rainer Haag*

ACS Applied Nano Materials, **2020,** Just Accepted Manuscript.

Author Contribution

Guy Guday designed the project, performed the synthesis and experiments, conducted characterization, and wrote the paper. Philip Nickl conducted follow-up characterization and helped edit the paper. Mohsen Adeli and Rainer Haag conceived the project, supervised the work, provided scientific guidance, and corrected the manuscript.

Reversible photothermal homogenization for fluorous biphasic systems with perfluoroalkylated nanographene

Guy Guday,[a] Mohsen Adeli*[ab] and Rainer Haag*[a]

Fluorous biphasic systems use the temperature-sensitive miscibility of fluorinated materials in non-fluorous solutions as a means to control reaction systems and easily separate catalysts or other compounds from a mixture. We present perfluoroalkylated nanographene as a viable platform for photo-homogenization and recycling of fluorous-tagged catalysts. Activation time and ease of recycling are both enhanced due to the graphene nanoconjugates.

Fluorous biphasic catalysis is a relatively well-established method for recovery and recycling of catalysts.[1-8] Catalyst recovery is important as the cost and toxicity of many widely used industrial catalysts gives increasing financial and environmental incentives to do so.[7] In order for a catalyst to be practically recoverable, it must be possible to collect a large fraction via simple techniques such as filtration or centrifugation and decantation. To be further recyclable, the collected catalyst must be purifiable while retaining its activity.[9, 10]

Highly fluorinated compounds show many unique properties and interactions; they are immiscible with aqueous solutions as well as most organic solvents, and exhibit strong fluorous-fluorous interactions.[3] While hydrophobicity is commonly thought of as implying lipophilicity and vice versa, fluorinated materials show both hydrophobic and lipophobic properties – meaning that water and many polar solvents as well as non-polar solvents do not wet fluorous surfaces.[2] Furthermore, the strong cohesive forces of fluorinated materials allows for the formation of a biphasic system under many circumstances.[1-3] The separation of fluorous phases from organic or aqueous phases has been shown to be temperature-sensitive, becoming miscible at elevated temperatures.[1, 3] Fluorous biphasic catalysis uses this controllable phase miscibility to introduce a catalyst to the non-fluorous phase upon heating, initiating the reaction. Subsequently, the mixed phases can be separated upon cooling, and the catalyst recovered and reused.

Horváth and Rábai first demonstrated the use of fluorous biphasic systems for targeted recovery of triphenylphosphine modified with perfluorinated chains when used with a fluorous solvent in addition to the hydrocarbon phase.[1] Since then, the field has been extensively researched, expanding the range of fluorous-tagged catalysts and evolving to include solid-state fluorous supports as an alternative to fluorous solvents.[11-13] The most common solid-state systems are centered around column chromatography with perfluoroalkylated silica gels.[5, 11-15] Due to the strong interactions between perfluorinated groups, separation of fluorinated and non-fluorinated material can be achieved with relatively high efficiency.[8, 16] However, there are still practical challenges with catalyst recovery by column chromatography, especially in the context of industrial-scale operations.[8, 10, 17]

Fluorous biphasic systems leverage the tunable phase separation of fluorinated and non-fluorinated compounds, most commonly by using perfluorocarbon chains conjugated to catalysts in order to enable controlled phase mixing and subsequent removal.[1, 5, 8, 9] This procedure can be used to recapture and recycle catalysts or ease purification. The use of fluorous solids rather than solvents can give rise to a solid-liquid fluorous biphasic system, whereby separation of the phases is simpler still as compared to a liquid-liquid system.[11-13, 15]

Graphene is a two-dimensional network of sp^2 conjugated carbon atoms, first discovered in 2004.[18] It has a range of unique and potentially useful properties, ranging from exceptional in-plane thermal and electronic conductivity[19] to high tensile strength and modulus,[20, 21] amongst others. Graphene also exhibits a photothermal effect, particularly in the near-infrared (NIR) range of the electromagnetic spectrum.[22-24] Unmodified graphene sheets are poorly dispersible in most solvents,[25] and while not exceptionally chemically reactive, there are a range of established methods for functionalizing graphene to produce 2D nanoplatforms.[20, 26-29] Functionalized graphene materials can take advantage of the inherent properties of graphene while benefiting from a carefully tuned surface chemistry to adjust intermolecular interactions.

[a] *Institut für Chemie und Biochemie, Freie Universität Berlin, Takustrasse 3, 14195 Berlin, Germany.*
[b] *Department of Chemistry, Faculty of Science, Lorestan University, Khorram Abad, 44316-68151 Iran.*

Electronic Supplementary Information (ESI) available: Experimental methods, NMR analysis, and additional data. See DOI: 10.1039/x0xx00000x

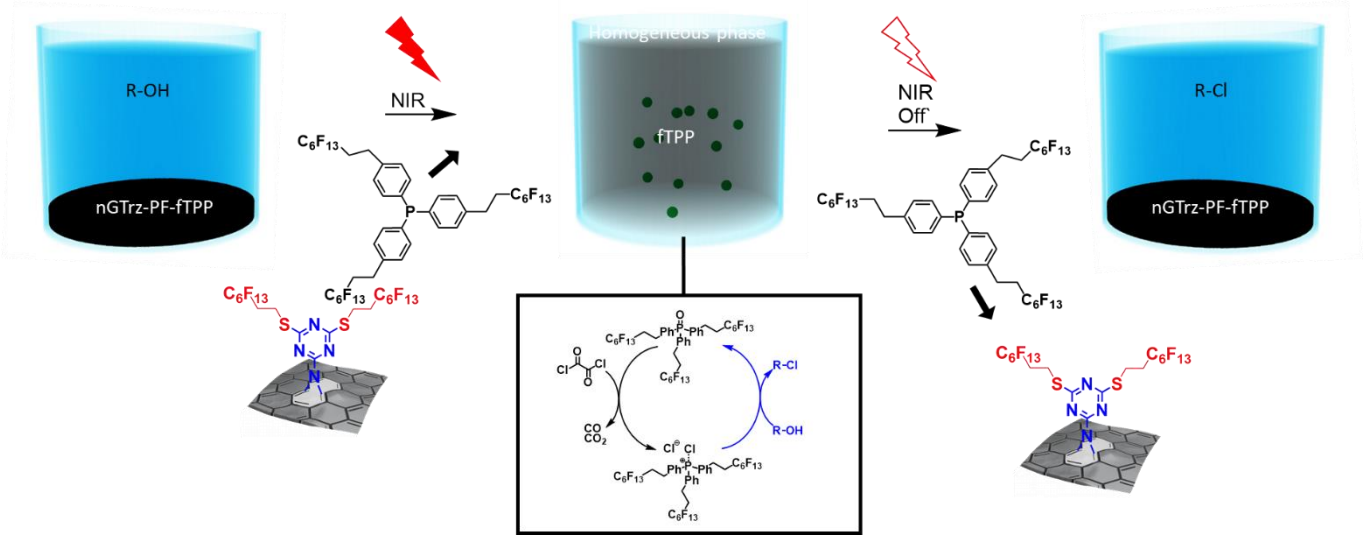

Figure 1. a) Scheme of catalyst release and homogenization in the nGTrz-PF solid-liquid biphasic system. Upon irradiation, fTPP catalyst is released and the system is homogenized through photothermal heating of nG. When irradiation is ceased, the fluorous phase aggregates upon cooling. b) Detailed mechanism of catalyst regeneration is shown in the callout.

In this work, we present a new solid-state fluorous platform based on a nanographene platform functionalized with a cyanuric chloride derivative (nGTrz) recently reported by our group.[30, 31] nGTrz was post-modified with 1H,1H,2H,2H-perfluoro-1-octanethiol (PF) to produce a fluorous 2D nanoplatform (nGTrz-PF) that exhibited photothermal heating, enabling photo-triggered phase miscibility with many liquid solvents. The nGTrz-PF platform showed a significant capacity for non-covalent loading of fluorous-tagged catalysts, yielding a system that offers precise control over phase transfer of catalysts as well as easy recovery and removal of the catalyst from a reaction mixture (**Figure 1a**). A catalytic Appel reaction (**Figure 1b,c**) with triphenylphosphine for halogenation of alcohols[32] was selected as a model reaction because fluorous-tagged triphenylphosphine (fTPP) is commercially available. Moreover, analysis of the reaction products was straight-forward, as the reactants and product can be quantitatively compared via NMR.

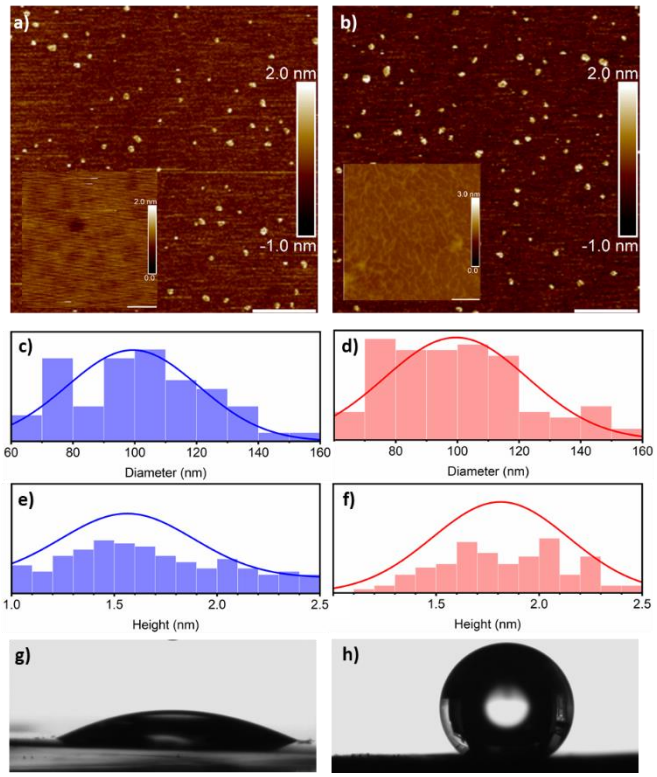

Figure 2. AFM images of a) nGTrz and b) nGTrz-PF with 1 µm scale bars, and insets showing detailed surface topography with 10 nm scale bars. Histograms of diameter for c) nGTrz and d) nGTrz-PF, and height for e) nGTrz and f) nGTrz-PF. Contact angle images of g) nGTrz and h) nGTrz-PF.

Post-modification of triazine-functionalized graphene derivatives have been shown to proceed in a facile, stepwise manner.[31, 33] The first chlorine reacts with nucleophiles near room temperature or at mildly elevated temperatures, while the second chlorine reacts at higher temperatures.[31] In this case, the reaction mixture containing nGTrz, catalytic quantities of triethylamine, was first heated to 40 °C for 24 hours and subsequently elevated to 80 °C for a further 24 hours, to maximize the degree of functionalization. Successful conjugation of PF and loading of the catalyst was investigated by atomic force microscopy (AFM), contact angle measurements, elemental analysis, and thermogravimetric analysis (TGA). Subsequently, the yield of the photo-induced Appel reactions was probed with NMR to determine conversion of the alcohol reagents over 10 cycles of catalysis and recycling.

AFM images (**Figure 2a,b**) show the relatively unchanged lateral dimensions of nGTrz and nGTrz-PF (**Figure 2c,d**) with averages of 99 nm ± 21 and 100 nm ± 23 respectively. However, the height increased upon perfluoroalkylation, from 1.56 nm ± 0.40 to 1.81 nm ± 0.33 (**Figure 2e,f**). The high-resolution insets (**Figure 2a,b**) showing the detailed surfaces of nGTrz and nGTrz-PF also display a clear addition of rough, ridge-like features in the latter, with apparent lengths on the range of 1 to 2 nm, which probably arise from the attached perfluorinated chains. Combined with contact angle measurements showing an increase from 28° ± 1.2 to 139° ± 1.7 upon perfluoroalkylation (**Figure 2g,h**), these results demonstrate a clear change in the height and surface properties of nGTrz-PF, attributed to successful conjugation of the perfluoroalkanes.

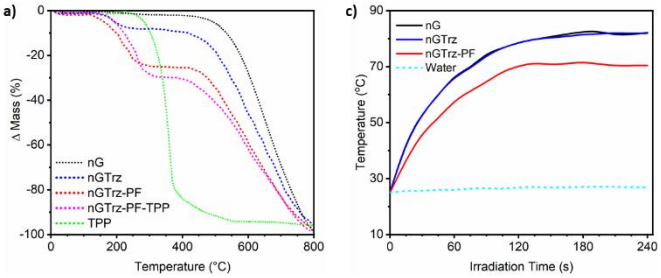

b)

	Element	wt.%
nGTrz	C	95.84
	H	0.06
	N	2.47
	S	0.05
	Other	1.58
nGTrz-PF	C	80.15
	H	0.40
	N	1.91
	S	1.85
	Other	15.69

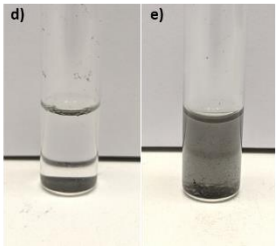

Figure 4. a) TGA thermograms for nG and other nanographene derivatives, along with fTPP. b) Elemental analysis results for nGTrz and nGTrz-PF. c) Photothermal heating curves for nG, nGTrz, nGTrz-PF, and water. nGTrz-PF in DCMde) before and e) after NIR irradiation, demonstrating photohomogenization.

Based on TGA results and elemental analysis (**Figure 3a**), nGTrz-PF contains approximately 1.8 PF chains per triazine moiety (Equation S1), corresponding to 90% of chlorine atoms having reacted, and about 20 wt.% of PF chains in this nanomaterial. TGA showed an additional mass loss of 19 wt.% for nGTrz-PF at 400 °C. At the same temperature nGTrz lost only 10 wt.% attributed to the triazine functional groups. Given that the PF chains themselves are thermally stable until significantly higher temperatures, this weight loss strongly suggests that the PF chains are covalently bound to triazine and thus are removed from the sample upon disintegration of that triazine functionality. The photothermal heating (**Figure 3b**) of nG and nGTrz is nearly identical, exceeding 80 °C within 3 minutes at a concentration of 1 mg/mL. nGTrz-PF shows a slightly subdued heating curve, reaching about 70 °C in 3 minutes. This can be largely attributed to the lower effective graphene concentration of nGTrz-PF, as PF chains make up nearly 20 wt.% of the material.

nGTrz-PF was loaded with up to about 15 wt.% of the fTPP catalyst according to TGA and CHN measurements, yielding nGTrz-PF-fTPP. The catalyst-loaded compound displayed a minimal decrease in loading over the course of multiple cycles of release and recapture. In contrast, nGTrz was only able to load under 2 wt.% of fTPP, although the catalyst could also be successively released and reloaded similarly to nGTrz-PF-fTPP. The dependence of loading on the presence of the PF chains, along with the near-complete release via NIR irradiation and reloading upon stopping irradiation, support the hypothesis that the perfluoroalkane groups of fTPP are able to bind non-covalently to the PF chains of nGTrz-PF via fluorous interactions, rather than a more general hydrophobic attraction.

A regenerative Appel reaction was used to test the ability of nGTrz-PF-fTPP to mediate NIR-induced catalyst homogenization. Catalyst (fTPP) released from nGTrz-PF-fTPP upon irradiation was chlorinated in situ by oxalyl chloride to be continuously regenerated (**Figure 1b**).[32] Initially, a series of six reactions were conducted, with: nGTrz-PF-fTPP, nGTrz-fTPP, and free fTPP – each reaction was conducted once under NIR irradiation, and once without. As shown by NMR (**Figure 4a**), 1-decanol was chlorinated only by nGTrz-PF-fTPP, and only when the reaction vessel was irradiated with an NIR lamp. Under all other conditions, only the side products of reaction between the alcohol and oxalyl chloride were produced.

After optimizing the reaction conditions, the recyclability of the nGTrz-PF-fTPP system was evaluated using 1-decanol and 3-phenyl-1-propanol as model reagents. In these experiments, nGTrz-PF-fTPP was reused for 10 successive reactions for each alcohol. In a process modified from the originally reported reaction, nGTrz-PF-fTPP and a small amount of oxalyl chloride were mixed in DCM for 15 minutes under NIR irradiation to release, homogenize, and activate the fTPP. Oxalyl chloride and the respective alcohol were then added dropwise over seven hours to the reaction mixture under continuous irradiation. Recycling of nGTrz-PF-fTPP was then performed by simply stopping NIR irradiation and allowing the reaction mixture to cool to room temperature, followed by centrifugation and washing, before being recharged with fresh reagents. NMR analysis (**Figure 4b,c**) showed similar reaction yields to those reported in the original catalytic Appel procedure,[32] at 85 % ± 3 for 1-chlorodecane and 54 % ± 7 for 3-phenyl-1-chloropropane, compared with reported yields of 83 % and 73 %, respectively. The yield decreased an average of 0.4 % ± 0.2 per cycle for 1-chlorodane and 2.2 % ± 0.5 for 3-phenyl-1-chloropropane over the course of 10 reactions (**Figure 4b**). The aromatic alcohol deviates substantially more from the reported values, although the yield in the first cycle was 65 %, which is much closer to the yield from the conventional reaction.

The recyclability and ease of separation for fluorous-tagged catalysts is a major reason for the interest they have generated. In this work we have shown that when used in conjugation with nGTrz-PF, these properties can be significantly enhanced. Separation and

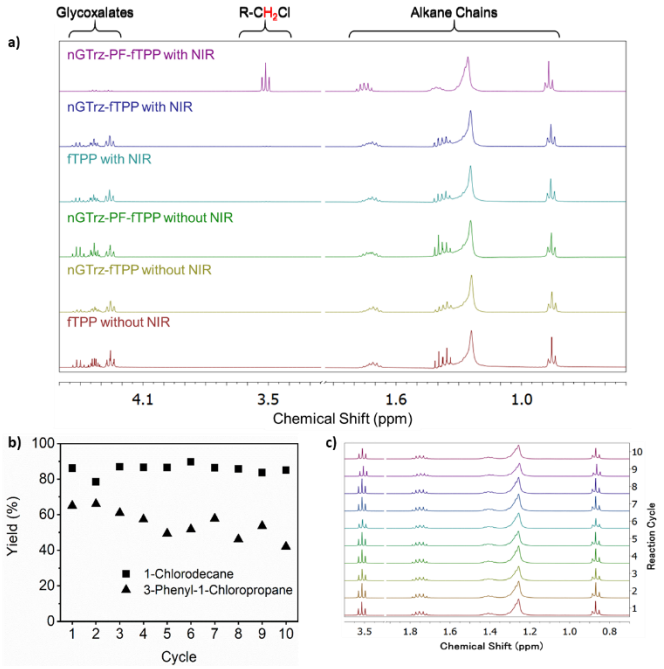

Figure 3. a) Abbreviated NMR spectra for decanol halogenation products with free fTPP and fTPP-loaded graphene derivatives, with and without NIR irradiation. b) Halogenation yield for 1-chlorodecane and 3-phenyl-1-chloropropane for 10 cycles with irradiation. c) Abbreviated NMR spectra of 1-chlorodecane over 10 reaction cycles with irradiation.

collection of fTPP were accomplished without the need for distillations, column techniques, or other time-consuming and potentially destructive methods. Instead, the solid fluorous phase could be isolated by centrifugation for reuse. Furthermore, photoresponsive, reversible homogenization of the fluorous and organic phases could be achieved within a short timeframe based on the photothermal heating properties of the nG component of the system. nGTrz-PF and similar derivatives could overcome some of the current practical limitations and drawbacks of both liquid-phase fluorous systems and other existing solid-phase systems, simplifying both the homogenization of fluorous catalysts as well as the recapture and purification of those catalysts.

The authors acknowledge the financial support of DFG Sonderforschungsbereich 1349 – Fluorine-specific Interactions, as well as Graduiertenkolleg 1582 – Fluorine as a Key Element. NMR measurements were performed by the Core Facility BioSupraMol at FU Berlin.

Conflicts of interest

There are no conflicts to declare.

Notes and references

1. I. T. Horvath and J. Rabai, *Science*, 1994, **266**, 72-75.
2. B. Cornils, *Angewandte Chemie International Edition in English*, 1997, **36**, 2057-2059.
3. E. de Wolf, G. van Koten and B.-J. Deelman, *Chemical Society Reviews*, 1999, **28**, 37-41.
4. J. A. Gladysz and D. P. Curran, *Tetrahedron*, 2002, **58**, 3823-3825.
5. C. C. Tzschucke, C. Markert, W. Bannwarth, S. Roller, A. Hebel and R. Haag, *Angew Chem Int Ed Engl*, 2002, **41**, 3964-4000.
6. S. J. Tavener and J. H. Clark, *Journal of Fluorine Chemistry*, 2003, **123**, 31-36.
7. M. Benaglia, *Recoverable and Recyclable Catalysts*, John Wiley & Sons, 1 edn., 2009.
8. B. Barabas, O. Fulop, R. Molontay and G. Palyi, *Acs Sustainable Chemistry & Engineering*, 2017, **5**, 8108-8118.
9. J. M. Vincent, *Chem Commun (Camb)*, 2012, **48**, 11382-11391.
10. J.-M. Vincent, M. Contel, G. Pozzi and R. H. Fish, *Coordination Chemistry Reviews*, 2019, **380**, 584-599.
11. M. Wende, R. Meier and J. A. Gladysz, *Journal of the American Chemical Society*, 2001, **123**, 11490-11491.
12. C. C. Tzschucke, C. Markert, H. Glatz and W. Bannwarth, *Angewandte Chemie-International Edition*, 2002, **41**, 4500-+.
13. A. Garcia-Bernabe, C. C. Tzschucke, W. Bannwarth and R. Haag, *Adv Synth Catal*, 2005, **347**, 1389-1394.
14. M. Wende and J. A. Gladysz, *Journal of the American Chemical Society*, 2003, **125**, 5861-5872.
15. K. L. O'Neal, H. Zhang, Y. Yang, L. Hong, D. Lu and S. G. Weber, *J Chromatogr A*, 2010, **1217**, 2287-2295.
16. C. Liu, X. Li and Z. Jin, *Catalysis Today*, 2015, **247**, 82-89.
17. W. Zhang, in *Green Techniques for Organic Synthesis and Medicinal Chemistry*, 2018, DOI: 10.1002/9781119288152.ch19, pp. 509-538.
18. K. S. Novoselov, A. K. Geim, S. V. Morozov, D. Jiang, Y. Zhang, S. V. Dubonos, I. V. Grigorieva and A. A. Firsov, *Science*, 2004, **306**, 666-669.
19. X. Li, W. Cai, J. An, S. Kim, J. Nah, D. Yang, R. Piner, A. Velamakanni, I. Jung, E. Tutuc, S. K. Banerjee, L. Colombo and R. S. Ruoff, *Science*, 2009, **324**, 1312-1314.
20. T. Ramanathan, A. A. Abdala, S. Stankovich, D. A. Dikin, M. Herrera-Alonso, R. D. Piner, D. H. Adamson, H. C. Schniepp, X. Chen, R. S. Ruoff, S. T. Nguyen, I. A. Aksay, R. K. Prud'Homme and L. C. Brinson, *Nat Nanotechnol*, 2008, **3**, 327-331.
21. M. Fang, K. Wang, H. Lu, Y. Yang and S. Nutt, *Journal of Materials Chemistry*, 2009, **19**.
22. Z. M. Markovic, L. M. Harhaji-Trajkovic, B. M. Todorovic-Markovic, D. P. Kepić, K. M. Arsikin, S. P. Jovanović, A. C. Pantovic, M. D. Dramićanin and V. S. Trajkovic, *Biomaterials*, 2011, **32**, 1121-1129.
23. K. Yang, L. Feng, X. Shi and Z. Liu, *Chem Soc Rev*, 2013, **42**, 530-547.
24. L. Feng, L. Wu and X. Qu, *Adv Mater*, 2013, **25**, 168-186.
25. Y. Hernandez, V. Nicolosi, M. Lotya, F. M. Blighe, Z. Sun, S. De, I. T. McGovern, B. Holland, M. Byrne, Y. K. Gun'Ko, J. J. Boland, P. Niraj, G. Duesberg, S. Krishnamurthy, R. Goodhue, J. Hutchison, V. Scardaci, A. C. Ferrari and J. N. Coleman, *Nat Nanotechnol*, 2008, **3**, 563-568.
26. V. Georgakilas, A. B. Bourlinos, R. Zboril, T. A. Steriotis, P. Dallas, A. K. Stubos and C. Trapalis, *Chem Commun (Camb)*, 2010, **46**, 1766-1768.
27. K. Suggs, D. Reuven and X.-Q. Wang, *The Journal of Physical Chemistry C*, 2011, **115**, 3313-3317.
28. V. Georgakilas, M. Otyepka, A. B. Bourlinos, V. Chandra, N. Kim, K. C. Kemp, P. Hobza, R. Zboril and K. S. Kim, *Chem Rev*, 2012, **112**, 6156-6214.
29. M. Quintana, E. Vazquez and M. Prato, *Acc Chem Res*, 2013, **46**, 138-148.
30. G. Guday, I. S. Donskyi, M. F. Gholami, G. Algara-Siller, F. Witte, A. Lippitz, W. E. S. Unger, B. Paulus, J. P. Rabe, M. Adeli and R. Haag, *Small*, 2019, DOI: 10.1002/smll.201805430, e1805430.
31. A. Faghani, I. S. Donskyi, M. Fardin Gholami, B. Ziem, A. Lippitz, W. E. Unger, C. Bottcher, J. P. Rabe, R. Haag and M. Adeli, *Angew Chem Int Ed Engl*, 2017, **56**, 2675-2679.
32. R. M. Denton, J. An and B. Adeniran, *Chem Commun (Camb)*, 2010, **46**, 3025-3027.
33. M. F. Gholami, D. Lauster, K. Ludwig, J. Storm, B. Ziem, N. Severin, C. Böttcher, J. P. Rabe, A. Herrmann, M. Adeli and R. Haag, *Advanced Functional Materials*, 2017, **27**, 1606477.

Reversible photothermal homogenization for fluorous biphasic systems with perfluoroalkylated nanographene

Guy Guday,[a] Mohsen Adeli[ab] and Rainer Haag*[a]

[a.] Institut für Chemie und Biochemie, Freie Universität Berlin, Takustrasse 3, 14195 Berlin, Germany.
[b.] Department of Chemistry, Faculty of Science, Lorestan University, Khorram Abad, 44316-68151 Iran.

Supporting Information

1. Experimental Methods

Materials
Graphite powder, median diameter 7-10 microns, and sodium azide (99%) were purchased from ACROS Organics. Sodium hypochlorite (11-14% available chlorine), 2,4,6-trichloro-1,3,5-triazine (99%), 3,3,4,4,5,5,6,6,7,7,8,8,8-Tridecafluoro-1-octanethiol (97%), triethylamine (>99%), Tris[4-(3,3,4,4,5,5,6,6,7,7,8,8,8-tridecafluorooctyl)phenyl]phosphine (>90%), 1-decanol (98%), and 3-phenyl-1-propanol (98%) were purchased from Sigma Aldrich. Water was derived from a Milli-Q advantage A10 water purification system in all experiments. All chemical compounds were used without further purification.

Production of nanographene (nG)
Graphite powder (1 g, ACROS Organics) was dispersed in a solution of as-received sodium hypochlorite (10 ml, 15% available chlorine, Sigma-Aldrich) and deionized water (10 ml). The dispersion was heated to 40 °C and stirred for 7 days. Then the mixture was purified by repeated centrifugation (typically 4 times, 10,000 rpm, 30 minutes) and then washed with water until the pH of the supernatant was neutral. Sonication was performed for 90 min to exfoliate the nanographene using a Bandolin Sonorex RK510H with a nominal frequency of 35 kHz and nominal power of 160 W. The solution was left overnight, then the supernatant was collected and centrifuged at 2000 rpm to remove remaining multilayer sheets or suspended graphite particles. The product was then lyophilized. Yield was 30% for ≤ 5 layers of nG, 15% for ≤ 2 layers of nG.

Synthesis of triazine-functionalized graphene (nGTrz)
2,4,6-trichloro-1,3,5-triazine (10 g, 54 mmol) was dissolved in N-methyl-2-pyrrolidone (100 ml) in a 500 ml single-neck, round-bottom flask and cooled down to 0 °C in an ice bath. Then sodium azide (3.52 g, 54 mmol) was added into the above solution upon stirring. In another flask, nG (300 mg) was dispersed in N-methyl-2-pyrrolidone (20 ml) and sonicated for 30 minutes. Then it was stirred for 30 minutes in an ice bath. 2,4,6-trichloro-1,3,5-triazine/sodium azide mixture was added into the nG dispersion and stirred for 1 hour at 0 °C. The ice bath was removed to allow the mixture to reach room temperature. Afterwards, the mixture was stirred at 70 °C for 12 h. The reaction mixture was sonicated for several minutes' intervals while it was stirring. The reaction mixture was cooled down

and pelleted and resuspended by centrifugation 3 times each in methanol, acetone, and distilled water. The mixture was then dialyzed against water for 3 days and freeze-dried. Yield was 95%.

Synthesis of nGTrz-PF

50 mg of nGTrz and 20 µL of triethylamine were dispersed in 10 g of Tridecafluoro-1-octanethiol, in a 50 mL round bottomed flask with a magnetic stir bar under nitrogen gas. The mixture was stirred at 400 rpm and heated first to 40°C for 24 hours, and then to 80°C for an additional 24 hours. Unreacted Tridecafluoro-1-octanethiol was removed by repeated centrifugation at 9000 rpm and washing with THF.

Preparation of nGTrz-PF-fTPP

In order to load the fluorous-tagged TPP onto nGTrz-PF, 50 mg of nGTrz-PF was dispersed in a solution of 100 mL THF and 20 mL of deionized water, while stirring at 600 rpm. Catalyst was then added in excess. The mixture was allowed to stir for 3 hours. At that point it was dialyzed against the same solvent mixture, with 5 kDa cutoff weight dialysis tubes, changed frequently. After 5 days of dialysis, the remaining solids were centrifuged and washed with deionized water until no organic solvents were left, and then lyophilized.

Modified Catalytic Appel Reaction

A hydrosun® 750 lamp with a 775W (Hydrosun Medizintechnik GmbH, Germany) nominal output in the red/near infrared range was used to irradiate all reactions.

Atomic Force Microscopy (AFM)

Samples were prepared by spin casting dispersions of graphene materials (0.1 mg ml^{-1}) in deionized water onto freshly cleaved mica substrates at 50 rps for 60 seconds. The mica substrates were mounted onto Ø12 mm stainless steel discs with double-sided tape. Measurements were performed using a Bruker Multimode 8, Nanoscope 5 with a J-type scanner, operated in tapping mode with Nanosensors PPP-NCLR cantilever tips with a typical resonant frequency of 190 kHz, a spring constant of 48 N m^{-1}, and a tip radius of < 10 nm. Images were recorded at a minimum resolution of 1024 x 1024 and a scan speed of 0.8 Hz or lower. All experiments were conducted under ambient conditions, and results were analyzed using the Bruker NanoScope Analysis 1.8 software, along with Gwyddion. Images were line-flattened using a first order (linear) fit.

Contact Angle Measurements

Contact angle with water was measured using an OCA contact angle goniometer system (DataPhysics Instruments, Germany). A 2 µL droplet of Milli-Q water was placed on the sample with the sessile drop method and equilibrated for 10s at room temperature. 10 points were measured for each sample and then averaged to get a reliable value.

TGA Measurements

Thermogravimetric analysis (TGA) was recorded on an STA PT 1600 Linseis (Robbinsville, USA) and evaluated with Linseis Data Acquisition software. The measurements were performed in aluminum oxide crucibles at temperatures ranging from 25 to 800 °C with a heating rate of 5 °C/min, under air.

Elemental Analysis

Elemental analysis was carried out on a VARIO EL III instrument (Elementar, Hanau, Germany) using sulfanilic acid as the standard.

Photothermal Heating
Photothermal properties of the material were measured using near-infrared (NIR) irradiation with a wavelength of λ = 785 nm at 500 mW cm^{-2}. For all experiments, 200 µl of aqueous solutions with 0.05 mg/ml of analyte were used, in 0.5 ml Eppendorf tubes.

NMR Measurements
1H NMR spectra were recorded using a Bruker DPX 400 MHz spectrometer using TMS as the internal standard.

Fourier transform infrared spectroscopy (FT-IR)
IR spectra were recorded using a JASCO 4100 spectrometer. Samples were measured as dry powders, with 48 accumulations and a resolution of 1 cm^{-1}.

2. Elemental Analysis Calculations

nGTrz
Triazine content was calculated based on nitrogen content. nG with no triazine groups has no measurable nitrogen content, while the triazine functionality conjugated onto graphene will contain 4 nitrogen atoms (3 in the ring and one from the nitrene), 3 carbon atoms (all in the ring), and 2 chlorine atoms. It is important to distinguish the carbon content of the Trz groups (C_{Trz}) as compared to that of nG (C_{nG}) when calculating functionalization density (FD) in terms of number of graphene carbon atoms per functional group. These procedures are shown below, based on the measured results for nGTrz, of 95.84 wt.% C and 2.47 wt.% N (**Figure 3b**). For ease of calculation, a theoretical sample mass of 100 atomic mass units (u).

$$N = \frac{2.47}{14} = 0.17$$

$$Trz = \frac{N}{4} = 0.044$$

$$C_{Trz} = Trz \times 3 = 0.132$$

$$FD = \frac{C_{nG}}{Trz\ groups} = \frac{(\frac{95.84}{12}) - 0.132}{0.044} = 178$$

nGTrz-PF
Upon perfluoroalkylation, PF content was calculated based on the sulfur content, assuming that newly added sulfur arises from the thioether bond between PF and Trz. The theoretically expected carbon content from nGTrz was determined by direct normalization of the value from nGTrz (above) based

on the nitrogen content in nGTrz-PF, and the total carbon content of nGTrz-PF compared with this value and the expected carbon content from the PF chains, as determined from Sulfur. Similarly, the expected fluorine content of PF was compared against the mass not accounted for by carbon, hydrogen, nitrogen, and sulfur – again, normalized to remove any undetermined mass that would arise from the nGTrz component of the system. As above, a theoretical sample mass of 100 u was used for ease of calculation.

$$PF = S_{nGTrz-PF} - S_{nGTrz} = \frac{1.85 - 0.05}{32} = 0.056$$

$$C_{PF} = PF \times 8 = 0.45 \; (= 5.4 \; wt.\%)$$

$$F_{PF} = PF \times 13 = 0.73 \; (= 13.8 \; wt.\%)$$

$$C_{nGTrz} = \frac{95.84}{12} \times \frac{1.91}{2.47} = 6.18 \; (= 74.1 \; wt.\%)$$

The total carbon content as predicted in the above equations amounts to 79.5 wt.%, while the experimentally measured result was 80.15 wt.%. Similarly, the calculated fluorine content accounts for 13.8 wt.%, while 15.69 wt.% was not attributed to carbon, nitrogen, hydrogen, or sulfur in the experimental results. The remaining unattributed mass can be attributed to oxygen and other atoms arising from nGTrz, as well as any newly added oxygen functionalities, for instance from any hydrolyzed chlorines of nGTrz.

3. NMR Analysis

As discussed in the main text, the chlorination of both 1-decanol and 3-phenyl-1-propanol could be easily followed by NMR. In the case of 1-decanol, there arise a series of peaks at upwards of 4.1 ppm which can be attributed to hydrogen atoms adjacent to glyoxylate. At 3.5 ppm, chlorine-adjecent hydrogens appear, while multiple signals between 0.8 and 1.8 ppm arise from the remaining alkyl hydrogens.[1] In the case of 3-phenyl-1-propanol, a similar set of signals arise, with a change in the alkyl region due to the short propyl chain and a new aromatic signal that is, thankfully, essentially unchanged before or after chlorination.

Integrals from the respective signals are presented below for each alcohol across 10 repeated reaction cycles (Table S1, Table S2), along with the calculated yield of their respective chlorides. Given the negligible amount of unconverted alcohol in all reactions (remaining oxalyl chloride is extremely reactive with alcohols), the yield was calculated simply as follows:

$$Yield = \frac{Cl \; integral}{Cl \; integral + Glyoxylate \; integral}$$

Table S1. NMR integrals and calculated reaction yields for 1-decanol chlorination

Reaction #	*Cl Integral*	*Glyoxylate Integral*	*Yield*
1	5.54	0.98	86
2	4.38	0.86	74
3	5.92	0.99	87
4	6.29	1.00	87
5	8.06	0.93	87
6	6.35	0.99	90
7	6.28	0.97	86
8	6.72	1.01	86
9	2.75	0.99	84
10	5.53	0.89	85

Table S2. NMR integrals and calculated reactions yields for 3-phenyl-1-propanol chlorination

Reaction #	*Cl Integral*	*Glyoxylate Integral*	*Yield*
1	0.26	0.14	65
2	0.22	0.18	55
3	0.25	0.16	61
4	1.60	1.19	57
5	1.67	1.71	49
6	1.61	1.50	52
7	1.52	1.11	58
8	0.18	0.21	46
9	1.70	1.47	54
10	1.54	2.12	42

3. Additional Results

The photothermal heating of aqueous solutions (0.05 g/ml) of nG, nGTrz, and nGTrz-PF were measured to demonstrate the feasibility of thermal-induced miscibility of the system (Figure S1). In all cases, temperatures had generally stabilized within four minutes, with peak temperatures of nearly 85 °C for nG and nGTrz, and over 70 °C for nGTrz-PF. This discrepancy could arise due to the lower overall graphene content of nGTrz-PF as compared to the other samples.

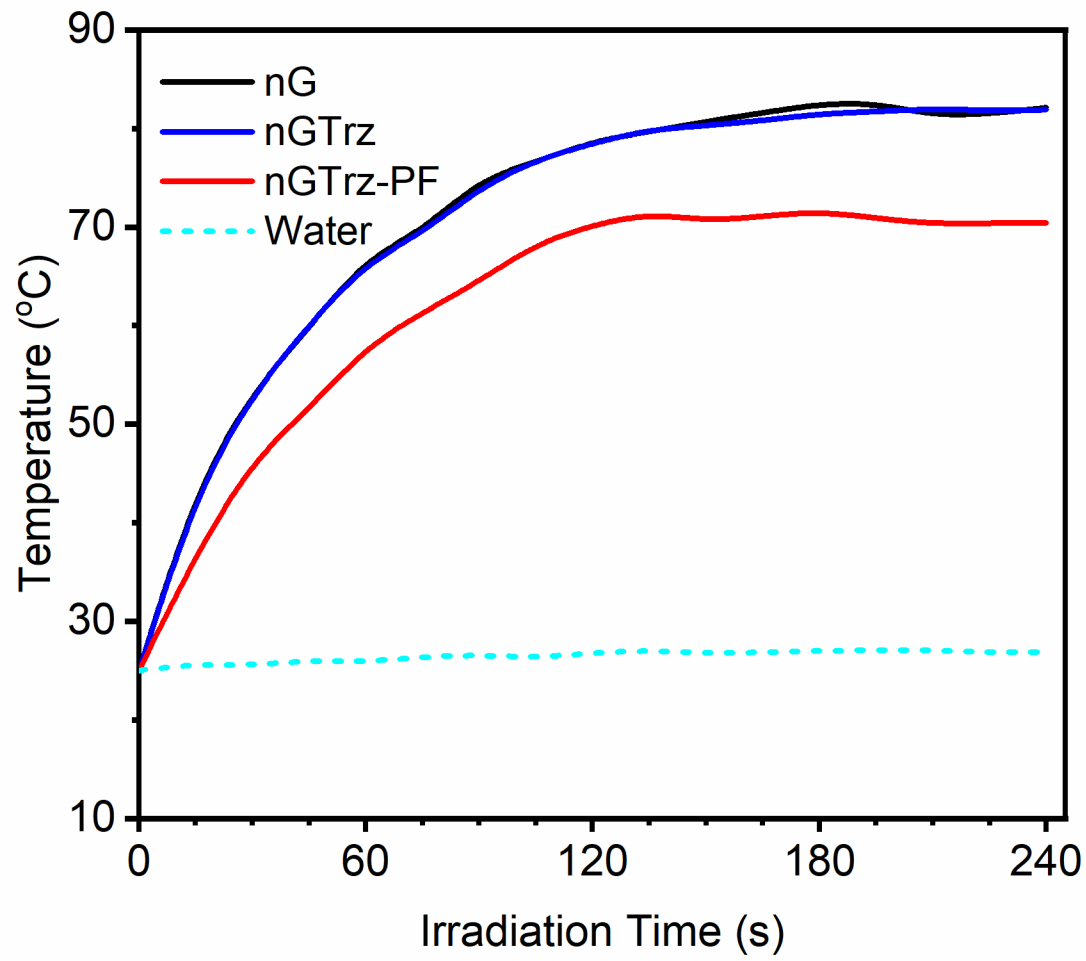

Figure S1. Photothermal heating curves of nG (black), nGTrz (blue), and nGTrz-PF (red) with plain water as a negative control.

References

[1] R. M. Denton, J. An, B. Adeniran, *Chem Commun (Camb)* **2010**, *46*, 3025-3027.

4 Summary and Outlook

In this work, a new method to produce nanographene was identified. The comparably high yield, scalability of a wet chemistry approach, and good quality of produced nG – defined in this case as narrow distributions of lateral size, low levels of sp^3 defects, and low number of layers – all provide significant benefits as compared to previously reported methodologies. The functionalization of these nG materials via [2+1] cycloaddition with Trz was carried out, and the resulting nGTrz material characterized in detail. nGTrz was found to exhibit behavior analogous to heteroatom doped graphene, namely *p*-type doping effects, whereby conductivity was increased. Combined with theoretical simulations, a new structure was proposed for the nitrene cycloaddition product of Trz with nG, with extensive supporting evidence in the form of statistical Raman and SFM-TM analysis.

The nGTrz platform was put into use by post-functionalization with short perfluoroalkanes, yielding a photothermally active fluorinated solid. The applications of this nGTrz-PF nanoconjugate for fluorous biphasic catalysis were explored and successfully demonstrated with fTPP in a modified regenerative Appel reaction, whereby alcohols could be chlorinated and the fTPP catalyst successfully reused with only minimal losses in efficacy over a minimum of 10 reactions.

Going forward, one of the primary benefits of nG is the small and very narrow size range of the sheets. For biological applications, especially drug delivery, this could be particularly relevant as the sheets can benefit from the EPR effect for tumor targeting. [8,123-124] Simultaneously, biomedical nanomaterials require very defined architectures for both consistent practical effect and regulatory approval – another area where nG could be advantageous compared to typical routes for producing graphenic materials.

The modified nGTrz system is more intriguing still, especially with the demonstrated electronic effects of Trz conjugation. The possibility of graphene's superaromatic network being able to incorporate at least the nitrogen bridge at the conjugation site, and perhaps the entire Trz moiety, raises a number of avenues for further exploration. Trz conjugation could prove to be a powerful method for band gap tuning of conductive or semi-conductive carbon nanomaterials, offering new routes for nanoelectronics. If the entire Trz ring is also incorporated into the electronic structure of nGTrz, vast possibilities arise for conductive networked materials. nGTrz crosslinked with aromatic moieties could yield 3D graphene composites with high isotropic conductivities. Similarly, conductive polymers with end groups targeting specific cells, pathogens, or molecules could be attached to nGTrz to produce highly sensitive graphene-based sensors.

Fluorous chemistry could also be explored further with nGTrz-PF. It will be worthwhile to investigate additional and potentially more powerful fluorinated catalysts as payloads, and also to explore the properties and potential new applications of similar nanosystems with higher degrees of functionalization. Increasing fluorine content is known to impact a range of material properties, including electronic properties and interfacial chemistry or interactions. Heavily fluorinated nG platforms could enable the production of photo-controllable superhydrophobic and lipophobic coatings, for instance, whereby a film of nG with more dense coverage of Trz and PF should be prepared. Given the temperature sensitive interfacial forces between fluorinated chains and other liquids, the photothermal heating of the nG component could allow controlled, temporary wettability.

5 Kurzzusammenfassung

Im Rahmen dieser Doktorarbeit, wurde eine neue Methode für die Synthese von Nanographen entwickelt. Der Prozess bietet eine vergleichsweise hohe Ausbeute, kann leicht hochskaliert werden, und produziert nG mit hervorragender Qualität; bei dieser Methode wird nur ein schmales Spektrum von Schichthöhe sowie Durchmesser erhalten, zusätzlich entstehen während der Produktion nur wenige sp^3 Defekte. Die bisher bekannten herkömmlichen Methoden bieten diese Vorteile nicht. Die Funktionalisierung dieser nG Materialien mit [2+1] Cycloaddition von Trz wurde durchgeführt, und das produzierte nGTrz sorgfältig charakterisiert. nGTrz zeigte hier ähnliche Eigenschaften wie *p*-type Heteroatom-dotiertes Graphen, die elektronische Leitfähigkeit ist für beide Schichten erhöht. Basierend auf experimentellen Ergebnissen mit Raman und Rasterkraftmikroskopie in Kombination mit theoretischen Simulationen, wurde eine neue Struktur für das Cycloadditionsprodukt von Trz mit nG bewiesen.

Das nGTrz System wurde mit Perfluoralkane modifiziert, um die Anwendungen des photothermisch-aktiv fluorierten Feststoff zu erforschen. Dieses nGTrz-PF Nanomaterial wurde zusammen mit fTPP zur fluorierten zwei-phasigen Katalyse erfolgreich eingesetzt. Das System konnte durch eine modifizierte Appel Reaktion Alkohole chlorieren. Der Katalysator konnte danach sogar aufgearbeitet und nahezu ohne Verlust auf das Ergebnis wieder eingesetzt werden. Die Lebensdauer erträgt mindestens zehn Reaktionszyklen.

In der Zukunft wird die geringe Größe von nG, vor allem kombiniert mit der reduzierten Segmentierung bzgl. der tatsächlichen Größen von großen Vorteil sein. Vor allem im biomedizinischem Bereich, speziell in der Wirkstofffreisetzung, ist eine Relevanz nicht von der Hand zu weisen. Graphen im Nanometerbereich kann durch den EPR-effekt besser in Tumore gelangen,[8,123-124] zusätzlich ist es – basierend auf den präziser definierten Geometrien – leichter nG zu benutzen, Derartige Variablen spielen auch in den Biointeraktionen schon eine eindeutig Rolle, und sind zurecht signifikant in regulativen Prozessen. Typische Graphenverfahren können diese zwei Punkte nicht erfüllen, was auch die Aufnahme von Graphen in die biopharmazeutische Sphäre verhindert.

Das modifizierte nGTrz System ist noch interessanter, vor allem die schon bekannte elektronische Wirkung der Trz-Konjugation. Es ist denkbar, dass das superaromatische Netzwerk von Graphen sich mindestens über die Stickstoffbrücke an die Trz-Verbindung ausbreitet, eventuell sogar über das gesamte Trz-Molekül. Beide Varianten würden neue Optionen für die weitere Forschung eröffnen. Die Trz-Konjugation könnte eine flexible Methode werden, die elektronischen Eigenschaften von leitfähigen oder Halbleiter-

Materialien zu ändern. Dies würde neue Optionen in der Nanoelektronik eröffnen. Sollte das gesamte Trz-Ring-Molekül zukünftig in das elektronische Netz integriert werden, entstehen zusätzliche Optionen für leitfähig vernetzte Materialien. Weiterhin gibt es die Möglichkeit, nGTrz mit aromatischen Crosslinkers zu vernetzen, um isotropische und leitfähige Netzwerke zu produzieren. Eine weitere Richtung wäre es, leitfähige Polymere mit Funktionalitäten die spezifische Wechselwirkungen für bestimmte Zellen wie Pathogene oder Moleküle zeigen,[75,222-223] mit nGTrz zu verbinden. So könnten hochsensible Sensoren produziert werden, die über das Gesamtsystem Signaländerungen messen können, die durch spezifische Interaktionen entstehen.

Fluorkatalyse kann auch mit nGTrz-PF weiterentwickelt werden. Es wäre lohnenswert, mehrere und möglicherweise an Bedeutung gewinnende fluorierte Katalysatoren statt fTPP auszuprobieren. Die Eigenschaften und potentiellen Anwendungen derartiger Nanosysteme mit höherem Funktionalisierungsgrad könnten auch interessant sein. Es ist bereits bekannt, dass höhere Fluor-Anteile einen Einfluss auf viele Materialeigenschaften haben. Unter anderem auch auf elektronische Eigenschaften und Oberflächen- und Grenzflächenchemie. Hochfluorierte nG-Plattformen könnten als Lichtstrahl-kontrollierte superhydrophobe sowie lipophobe Schichten dienen, wobei nG mit einem höheren Trz und dementsprechenden PF Anteil produziert werden müsste. Basiert auf der thermosensiblen Phasenchemie von fluorierten Materialien und nicht-fluorierten Flüssigkeiten sowie die zusätzlich zu bedenkenden photothermischen Eigenschaften des nG Anteils, erhält man am Ende Systeme, welche kontrollierbare temporäre Hydro- und Lipophilizität zeigen.

6 References

[1] A. C. Neto, F. Guinea, N. M. Peres, *Physics World* **2006**, *19*, v.

[2] T. Ramanathan, A. A. Abdala, S. Stankovich, D. A. Dikin, M. Herrera-Alonso, R. D. Piner, D. H. Adamson, H. C. Schniepp, X. Chen, R. S. Ruoff, S. T. Nguyen, I. A. Aksay, R. K. Prud'Homme, L. C. Brinson, *Nat Nanotechnol* **2008**, *3*, 327-331.

[3] Z. Xu, Y. Zhang, P. Li, C. Gao, *ACS Nano* **2012**, *6*, 7103-7113.

[4] F. Perreault, A. Fonseca de Faria, M. Elimelech, *Chem Soc Rev* **2015**, *44*, 5861-5896.

[5] K. S. Novoselov, A. K. Geim, S. V. Morozov, D. Jiang, Y. Zhang, S. V. Dubonos, I. V. Grigorieva, A. A. Firsov, *Science* **2004**, *306*, 666-669.

[6] X. Li, Y. Zhu, W. Cai, M. Borysiak, B. Han, D. Chen, R. D. Piner, L. Colombo, R. S. Ruoff, *Nano Lett* **2009**, *9*, 4359-4363.

[7] H. K. He, C. Gao, *Chemistry of Materials* **2010**, *22*, 5054-5064.

[8] W. Yang, C. He, L. Zhang, Y. Wang, Z. Shi, M. Cheng, G. Xie, D. Wang, R. Yang, D. Shi, G. Zhang, *Small* **2012**, *8*, 1429-1435.

[9] X. Yan, X. Cui, B. Li, L. S. Li, *Nano Lett* **2010**, *10*, 1869-1873.

[10] K. Yang, J. Wan, S. Zhang, B. Tian, Y. Zhang, Z. Liu, *Biomaterials* **2012**, *33*, 2206-2214.

[11] K. Yang, L. Feng, X. Shi, Z. Liu, *Chem Soc Rev* **2013**, *42*, 530-547.

[12] L. Sun, K. Frykholm, L. H. Fornander, S. Svedhem, F. Westerlund, B. Akerman, *J Phys Chem B* **2014**, *118*, 11895-11904.

[13] H. C. Schniepp, J. L. Li, M. J. McAllister, H. Sai, M. Herrera-Alonso, D. H. Adamson, R. K. Prud'homme, R. Car, D. A. Saville, I. A. Aksay, *J Phys Chem B* **2006**, *110*, 8535-8539.

[14] M. J. McAllister, J.-L. Li, D. H. Adamson, H. C. Schniepp, A. A. Abdala, J. Liu, M. Herrera-Alonso, D. L. Milius, R. Car, R. K. Prud'homme, I. A. Aksay, *Chemistry of Materials* **2007**, *19*, 4396-4404.

[15] H. W. Kroto, J. R. Heath, S. C. O'Brien, R. F. Curl, R. E. Smalley, *Nature* **1985**, *318*, 162-163.

[16] M. Arndt, O. Nairz, J. Vos-Andreae, C. Keller, G. van der Zouw, A. Zeilinger, *Nature* **1999**, *401*, 680-682.

[17] L. Zhou, C. Gao, D. Zhu, W. Xu, F. F. Chen, A. Palkar, L. Echegoyen, E. S. Kong, *Chemistry* **2009**, *15*, 1389-1396.

[18] M. R. Hamblin, *Photochemical & Photobiological Sciences* **2018**, *17*, 1515-1533.

[19] J. Catalan, J. Elguero, *Journal of the American Chemical Society* **1993**, *115*, 9249-9252.

[20] T. Soga, *Nanostructured materials for solar energy conversion.*, Elsevier, Amsterdam Boston, **2006**.

[21] X. Lu, Z. Chen, *Chemical Reviews* **2005**, *105*, 3643-3696.

[22] Z. Hu, C. Zhang, Y. Huang, S. Sun, W. Guan, Y. Yao, *Chemico-Biological Interactions* **2012**, *195*, 86-94.

[23] T. Nogami, M. Tsuda, T. Ishida, S. Kurono, M. Ohashi, *Fullerene Science and Technology* **1993**, *1*, 275-285.

[24] C. Bingel, *Chemische Berichte* **1993**, *126*, 1957-1959.

[25] M. Prato, Q. C. Li, F. Wudl, V. Lucchini, *Journal of the American Chemical Society* **1993**, *115*, 1148-1150.

[26] S. Yamago, H. Tokuyama, E. Nakamura, M. Prato, F. Wudl, *The Journal of Organic Chemistry* **1993**, *58*, 4796-4798.

[27] F. Diederich, C. Thilgen, *Science* **1996**, *271*, 317-323.

[28] Z. Beiranvand, A. Kakanejadifard, I. S. Donskyi, A. Faghani, Z. Tu, A. Lippitz, P. Sasanpour, F. Maschietto, B. Paulus, W. E. S. Unger, R. Haag, M. Adeli, *RSC Advances* **2016**, *6*, 112771-112775.

[29] I. Donskyi, K. Achazi, V. Wycisk, C. Bottcher, M. Adeli, *Chem Commun (Camb)* **2016**, *52*, 4373-4376.

[30] F. Diederich, L. Isaacs, D. Philp, *Journal of the Chemical Society, Perkin Transactions 2* **1994**.

[31] Y. Nakamura, M. Suzuki, Y. Imai, J. Nishimura, *Org Lett* **2004**, *6*, 2797-2799.

[32] T. Nakahodo, M. Okada, H. Morita, T. Yoshimura, M. O. Ishitsuka, T. Tsuchiya, Y. Maeda, H. Fujihara, T. Akasaka, X. Gao, S. Nagase, *Angew Chem Int Ed Engl* **2008**, *47*, 1298-1300.

[33] E. Yoo, J. Kim, E. Hosono, H. S. Zhou, T. Kudo, I. Honma, *Nano Lett* **2008**, *8*, 2277-2282.

[34] Y. Z. An, J. L. Anderson, Y. Rubin, *The Journal of Organic Chemistry* **1993**, *58*, 4799-4801.

[35] C. J. Hawker, K. L. Wooley, J. M. J. Fréchet, *J. Chem. Soc., Chem. Commun.* **1994**, 925-926.

[36] A. Hirsch, I. Lamparth, T. Groesser, H. R. Karfunkel, *Journal of the American Chemical Society* **1994**, *116*, 9385-9386.

[37] G. E. Ball, G. A. Burley, L. Chaker, B. C. Hawkins, J. R. Williams, P. A. Keller, S. G. Pyne, *J Org Chem* **2005**, *70*, 8572-8574.

[38] M. Abdolkarimi-Mahabadi, M. Manteghian, *Fullerenes, Nanotubes and Carbon Nanostructures* **2015**, *23*, 860-864.

[39] K. Huth, M. Glaeske, K. Achazi, G. Gordeev, S. Kumar, R. Arenal, S. K. Sharma, M. Adeli, A. Setaro, S. Reich, R. Haag, *Small* **2018**, *14*, e1800796.

[40] E. A. Laird, F. Kuemmeth, G. A. Steele, K. Grove-Rasmussen, J. Nygård, K. Flensberg, L. P. Kouwenhoven, *Reviews of Modern Physics* **2015**, *87*, 703-764.

[41] M. K. Bayazit, K. S. Coleman, *J Am Chem Soc* **2009**, *131*, 10670-10676.

[42] B. Peng, M. Locascio, P. Zapol, S. Li, S. L. Mielke, G. C. Schatz, H. D. Espinosa, *Nature Nanotechnology* **2008**, *3*, 626.

[43] M. Holzinger, O. Vostrowsky, A. Hirsch, F. Hennrich, M. Kappes, R. Weiss, F. Jellen, *Angewandte Chemie International Edition* **2001**, *40*.

[44] K. S. Coleman, S. R. Bailey, S. Fogden, M. L. Green, *J Am Chem Soc* **2003**, *125*, 8722-8723.

[45] S. Munirasu, J. Albuerne, A. Boschetti-de-Fierro, V. Abetz, *Macromol Rapid Commun* **2010**, *31*, 574-579.

[46] Y. Chen, A. Star, S. Vidal, *Chem Soc Rev* **2013**, *42*, 4532-4542.

[47] H. F. Bettinger, *Chemistry* **2006**, *12*, 4372-4379.

[48] M. Quintana, M. Grzelczak, M. Prato, *Physica Status Solidi B-Basic Solid State Physics* **2010**, *247*, 2645-2648.

[49] A. Criado, M. Vizuete, M. J. Gómez-Escalonilla, S. García-Rodriguez, J. L. G. Fierro, A. Cobas, D. Peña, E. Guitián, F. Langa, *Carbon* **2013**, *63*, 140-148.

[50] M. Eskandari, S. H. Hosseini, M. Adeli, A. Pourjavadi, *Iranian Polymer Journal* **2014**, *23*, 387-403.

[51] A. Setaro, M. Adeli, M. Glaeske, D. Przyrembel, T. Bisswanger, G. Gordeev, F. Maschietto, A. Faghani, B. Paulus, M. Weinelt, R. Arenal, R. Haag, S. Reich, *Nat Commun* **2017**, *8*, 14281.

[52] C. Gao, H. He, L. Zhou, X. Zheng, Y. Zhang, *Chemistry of Materials* **2009**, *21*, 360-370.

[53] Z. M. Markovic, L. M. Harhaji-Trajkovic, B. M. Todorovic-Markovic, D. P. Kepić, K. M. Arsikin, S. P. Jovanović, A. C. Pantovic, M. D. Dramićanin, V. S. Trajkovic, *Biomaterials* **2011**, *32*, 1121-1129.

[54] E. J. Lawrence, G. G. Wildgoose, L. Aldous, Y. A. Wu, J. H. Warner, R. G. Compton, P. D. McNaughter, *Chemistry of Materials* **2011**, *23*, 3740-3751.

[55] Vlasova, II, T. V. Vakhrusheva, A. V. Sokolov, V. A. Kostevich, A. A. Gusev, S. A. Gusev, V. I. Melnikova, A. S. Lobach, *Toxicol Appl Pharmacol* **2012**, *264*, 131-142.

[56] B. Wan, Z. X. Wang, Q. Y. Lv, P. X. Dong, L. X. Zhao, Y. Yang, L. H. Guo, *Toxicol Lett* **2013**, *221*, 118-127.

[57] L. M. Saeed, M. Mahmood, S. J. Pyrek, T. Fahmi, Y. Xu, T. Mustafa, Z. A. Nima, S. M. Bratton, D. Casciano, E. Dervishi, *Journal of Applied Toxicology* **2014**, *34*, 1188-1199.

[58] X. Liu, A. L. Miller, 2nd, S. Park, B. E. Waletzki, Z. Zhou, A. Terzic, L. Lu, *ACS Appl Mater Interfaces* **2017**, *9*, 14677-14690.

[59] B. C. Brodie, *Philosophical Transactions of the Royal Society of London* **1859**, *149*, 249-259.

[60] W. S. Hummers, R. E. Offeman, *Journal of the American Chemical Society* **1958**, *80*, 1339-1339.

[61] C. E. Halbig, T. J. Nacken, J. Walter, C. Damm, S. Eigler, W. Peukert, *Carbon* **2016**, *96*, 897-903.

[62] R. K. Layek, A. K. Nandi, *Polymer* **2013**, *54*, 5087-5103.

[63] S. Eigler, A. Hirsch, *Angew Chem Int Ed Engl* **2014**, *53*, 7720-7738.

[64] X. Li, W. Cai, J. An, S. Kim, J. Nah, D. Yang, R. Piner, A. Velamakanni, I. Jung, E. Tutuc, S. K. Banerjee, L. Colombo, R. S. Ruoff, *Science* **2009**, *324*, 1312-1314.

[65] Y. Hernandez, V. Nicolosi, M. Lotya, F. M. Blighe, Z. Sun, S. De, I. T. McGovern, B. Holland, M. Byrne, Y. K. Gun'Ko, J. J. Boland, P. Niraj, G. Duesberg, S. Krishnamurthy, R. Goodhue, J. Hutchison, V. Scardaci, A. C. Ferrari, J. N. Coleman, *Nat Nanotechnol* **2008**, *3*, 563-568.

[66] U. Khan, A. O'Neill, M. Lotya, S. De, J. N. Coleman, *Small* **2010**, *6*, 864-871.

[67] Y. T. Liang, M. C. Hersam, *J Am Chem Soc* **2010**, *132*, 17661-17663.

[68] L. Chen, Y. Hernandez, X. Feng, K. Müllen, *Angew Chem Int Ed Engl* **2012**, *51*, 7640-7654.

[69] A. Narita, X. Y. Wang, X. Feng, K. Müllen, *Chem Soc Rev* **2015**, *44*, 6616-6643.

[70] S. B. Singh, C. M. Hussain, *ChemistrySelect* **2018**, *3*, 9533-9544.

[71] S. H. Shim, K. T. Kim, J. U. Lee, W. H. Jo, *ACS Appl Mater Interfaces* **2012**, *4*, 4184-4191.

[72] R. Guo, L. Qi, Z. Mo, Q. Wu, S. Yang, *Iranian Polymer Journal* **2017**, *26*, 423-430.

[73] X. Sun, Z. Liu, K. Welsher, J. T. Robinson, A. Goodwin, S. Zaric, H. Dai, *Nano Res* **2008**, *1*, 203-212.

[74] L. Zhang, J. Xia, Q. Zhao, L. Liu, Z. Zhang, *Small* **2010**, *6*, 537-544.

[75] Z. Tu, G. Guday, M. Adeli, R. Haag, *Advanced Materials* **2018**, *30*, 1706709.

[76] J. Y. Hwang, C. C. Kuo, L. C. Chen, K. H. Chen, *Nanotechnology* **2010**, *21*, 465705.

[77] L. G. Cancado, A. Jorio, E. H. Ferreira, F. Stavale, C. A. Achete, R. B. Capaz, M. V. Moutinho, A. Lombardo, T. S. Kulmala, A. C. Ferrari, *Nano Lett* **2011**, *11*, 3190-3196.

[78] Z. Wang, X. Zhou, J. Zhang, F. Boey, H. Zhang, *The Journal of Physical Chemistry C* **2009**, *113*, 14071-14075.

[79] A. Ambrosi, C. K. Chua, N. M. Latiff, A. H. Loo, C. H. Wong, A. Y. Eng, A. Bonanni, M. Pumera, *Chem Soc Rev* **2016**, *45*, 2458-2493.

[80] Q. Mu, G. Su, L. Li, B. O. Gilbertson, L. H. Yu, Q. Zhang, Y.-P. Sun, B. Yan, *ACS applied materials & interfaces* **2012**, *4*, 2259-2266.

[81] O. Akhavan, E. Ghaderi, A. Akhavan, *Biomaterials* **2012**, *33*, 8017-8025.

[82] J. Shen, Y. Zhu, X. Yang, C. Li, *Chem Commun (Camb)* **2012**, *48*, 3686-3699.

[83] H. Ren, E. Cunha, Q. Sun, Z. Li, I. A. Kinloch, R. J. Young, Z. Fan, *Nanoscale Advances* **2019**.

[84] J. Tuček, P. Błoński, O. Malina, M. Pumera, C. K. Chua, M. Otyepka, R. Zbořil, *Advanced Functional Materials* **2018**, *28*, 1800592.

[85] T. Enoki, M. Kiguchi, *Physica Scripta* **2018**, *93*, 053001.

[86] D. Lungerich, O. Papaianina, M. Feofanov, J. Liu, M. Devarajulu, S. I. Troyanov, S. Maier, K. Amsharov, *Nature Communications* **2018**, *9*, 4756.

[87] M. Bacon, S. J. Bradley, T. Nann, *Particle & Particle Systems Characterization* **2014**, *31*, 415-428.

[88] C. Cheng, J. Zhang, S. Li, Y. Xia, C. Nie, Z. Shi, J. L. Cuellar-Camacho, N. Ma, R. Haag, *Adv Mater* **2018**, *30*.

[89] H. Cheng, K. Gadora, Z. Wang, H. Zhang, W. Jiang, X. Chen, G. Han, Y. Jin, J. Zhou, L. Jiang, Y. Ding, *Drug Discovery Today* **2019**, *24*, 749-762.

[90] M.-C. Matesanz, M. Vila, M.-J. Feito, J. Linares, G. Gonçalves, M. Vallet-Regi, P.-A. A. Marques, M.-T. Portolés, *Biomaterials* **2013**, *34*, 1562-1569.

[91] J. Linares, M. C. n. Matesanz, M. Vila, M. J. Feito, G. Gonçalves, M. Vallet-Regí, P. A. Marques, M. T. Portolés, *ACS applied materials & interfaces* **2014**, *6*, 13697-13706.

[92] S. M. Chowdhury, P. Manepalli, B. Sitharaman, *Acta biomaterialia* **2014**, *10*, 4494-4504.

[93] L. Candelaria, L. V. Frolova, B. M. Kowalski, K. Artyushkova, A. Serov, N. G. Kalugin, *Sci Rep* **2018**, *8*, 14747.

[94] Y. Zhu, X. Guo, Y. Li, J. Wang, *Journal of the American Chemical Society* **2019**, *141*, 5511-5517.

[95] X. Tan, Y. Li, X. Li, S. Zhou, L. Fan, S. Yang, *Chem Commun (Camb)* **2015**, *51*, 2544-2546.

[96] V. Georgakilas, J. N. Tiwari, K. C. Kemp, J. A. Perman, A. B. Bourlinos, K. S. Kim, R. Zboril, *Chem Rev* **2016**, *116*, 5464-5519.

[97] X. T. Zheng, A. Ananthanarayanan, K. Q. Luo, P. Chen, *Small* **2015**, *11*, 1620-1636.

[98] X. Zhou, S. Guo, P. Zhong, Y. Xie, Z. Li, X. Ma, *RSC Advances* **2016**, *6*, 54644-54648.

[99] A. D. Senese, W. A. Chalifoux, *Molecules* **2018**, *24*, 118.

[100] H.-A. Lin, Y. Sato, Y. Segawa, T. Nishihara, N. Sugimoto, L. T. Scott, T. Higashiyama, K. Itami, *Angewandte Chemie International Edition* **2018**, *57*, 2874-2878.

[101] D. Cortizo-Lacalle, J. P. Mora-Fuentes, K. Strutyński, A. Saeki, M. Melle-Franco, A. Mateo-Alonso, *Angewandte Chemie International Edition* **2018**, *57*, 703-708.

[102] S. Guo, S. Dong, *Chem Soc Rev* **2011**, *40*, 2644-2672.

[103] H. Zhang, C. Peng, J. Yang, M. Lv, R. Liu, D. He, C. Fan, Q. Huang, *ACS applied materials & interfaces* **2013**, *5*, 1761-1767.

[104] H. Medina, Y.-C. Lin, C. Jin, C.-C. Lu, C.-H. Yeh, K.-P. Huang, K. Suenaga, J. Robertson, P.-W. Chiu, *Advanced Functional Materials* **2012**, *22*, 2123-2128.

[105] T. Wu, X. Zhang, Q. Yuan, J. Xue, G. Lu, Z. Liu, H. Wang, H. Wang, F. Ding, Q. Yu, X. Xie, M. Jiang, *Nat Mater* **2016**, *15*, 43-47.

[106] G. Guday, I. S. Donskyi, M. F. Gholami, G. Algara-Siller, F. Witte, A. Lippitz, W. E. S. Unger, B. Paulus, J. P. Rabe, M. Adeli, R. Haag, *Small* **2019**, 1805430.

[107] D. W. Lee, T. Kim, M. Lee, *Chem Commun (Camb)* **2011**, *47*, 8259-8261.

[108] P. Lin, Y. Cong, C. Sun, B. Zhang, *Nanoscale* **2016**, *8*, 2403-2411.

[109] C. Sun, K. L. Walker, D. L. Wakefield, W. R. Dichtel, *Chemistry of Materials* **2015**, *27*, 4499-4504.

[110] A. Ghosh, K. V. Rao, S. J. George, C. N. R. Rao, *Chemistry – A European Journal* **2010**, *16*, 2700-2704.

[111] Y. Liu, H. Zhong, Y. Qin, Y. Zhang, X. Liu, T. Zhang, *RSC Advances* **2016**, *6*, 30184-30193.

[112] D. Y. Lee, Z. Khatun, J. H. Lee, Y. K. Lee, I. In, *Biomacromolecules* **2011**, *12*, 336-341.

[113] J. Liu, S. Guo, L. Han, T. Wang, W. Hong, Y. Liu, E. Wang, *Journal of Materials Chemistry* **2012**, *22*.

[114] A. Sahu, W. I. Choi, J. H. Lee, G. Tae, *Biomaterials* **2013**, *34*, 6239-6248.

[115] J. Li, N. Ren, J. Qiu, X. Mou, H. Liu, *Int J Nanomedicine* **2013**, *8*, 3415-3426.

[116] W. Qi, W. Yuan, J. Yan, H. Wang, *Journal of Materials Chemistry B* **2014**, *2*, 5461-5467.

[117] V. Georgakilas, M. Otyepka, A. B. Bourlinos, V. Chandra, N. Kim, K. C. Kemp, P. Hobza, R. Zboril, K. S. Kim, *Chem Rev* **2012**, *112*, 6156-6214.

[118] C. K. Chua, M. Pumera, *Chem Soc Rev* **2013**, *42*, 3222-3233.

[119] S. Mallakpour, A. Abdolmaleki, S. Borandeh, *Applied Surface Science* **2014**, *307*, 533-542.

[120] H. Bao, Y. Pan, Y. Ping, N. G. Sahoo, T. Wu, L. Li, J. Li, L. H. Gan, *Small* **2011**, *7*, 1569-1578.

[121] G. Xu, X. Chen, J. Hu, P. Yang, D. Yang, L. Wei, *Analyst* **2012**, *137*, 2757-2761.

[122] Y. Pan, H. Bao, N. G. Sahoo, T. Wu, L. Li, *Advanced Functional Materials* **2011**, *21*, 2754-2763.

[123] Z. Liu, J. T. Robinson, X. Sun, H. Dai, *J Am Chem Soc* **2008**, *130*, 10876-10877.

[124] K. Yang, J. Wan, S. Zhang, Y. Zhang, S. T. Lee, Z. Liu, *ACS Nano* **2011**, *5*, 516-522.

[125] L. Feng, X. Yang, X. Shi, X. Tan, R. Peng, J. Wang, Z. Liu, *Small* **2013**, *9*, 1989-1997.

[126] J. Chen, H. Liu, C. Zhao, G. Qin, G. Xi, T. Li, X. Wang, T. Chen, *Biomaterials* **2014**, *35*, 4986-4995.

[127] Y. Zeng, Z. Yang, S. Luo, H. Li, C. Liu, Y. Hao, J. Liu, W. Wang, R. Li, *RSC Advances* **2015**, *5*, 57725-57734.

[128] S. Reshma, S. Syama, P. Mohanan, *Colloids and Surfaces B: Biointerfaces* **2016**, *140*, 104-116.

[129] K. Yang, S. Zhang, G. Zhang, X. Sun, S.-T. Lee, Z. Liu, *Nano Letters* **2010**, *10*, 3318-3323.

[130] H. K. Cheng, N. G. Sahoo, Y. P. Tan, Y. Pan, H. Bao, L. Li, S. H. Chan, J. Zhao, *ACS Appl Mater Interfaces* **2012**, *4*, 2387-2394.

[131] C.-W. Lo, D. Zhu, H. Jiang, *Soft Matter* **2011**, *7*.

[132] C. Shan, H. Yang, D. Han, Q. Zhang, A. Ivaska, L. Niu, *Langmuir* **2009**, *25*, 12030-12033.

[133] H. Yang, F. Li, C. Shan, D. Han, Q. Zhang, L. Niu, A. Ivaska, *Journal of Materials Chemistry* **2009**, *19*.

[134] J. Han, Y. Shen, W. Feng, *Nanoscale* **2016**, *8*, 14139-14145.

[135] C. K. Chua, Z. Sofer, J. Luxa, M. Pumera, *Chemistry - A European Journal* **2015**, *21*, 7969-7969.

[136] H. Wang, Q. Zhang, X. Chu, T. Chen, J. Ge, R. Yu, *Angewandte Chemie International Edition* **2011**, *50*, 7065-7069.

[137] C. K. Chua, M. Pumera, *ACS Nano* **2015**, *9*, 4193-4199.

[138] M. Prato, T. Suzuki, H. Foroudian, Q. Li, K. Khemani, F. Wudl, J. Leonetti, R. D. Little, T. White, *Journal of the American Chemical Society* **1993**, *115*, 1594-1595.

[139] M. Cases, M. Duran, M. Sol, *Journal of Molecular Modeling* **2000**, *6*, 205-212.

[140] V. Georgakilas, A. B. Bourlinos, R. Zboril, T. A. Steriotis, P. Dallas, A. K. Stubos, C. Trapalis, *Chem Commun (Camb)* **2010**, *46*, 1766-1768.

[141] M. Quintana, K. Spyrou, M. Grzelczak, W. R. Browne, P. Rudolf, M. Prato, *ACS Nano* **2010**, *4*, 3527-3533.

[142] K. Suggs, D. Reuven, X.-Q. Wang, *The Journal of Physical Chemistry C* **2011**, *115*, 3313-3317.

[143] P. A. Denis, F. Iribarne, *Journal of Materials Chemistry* **2012**, *22*.

[144] P. A. Denis, *Chemistry* **2013**, *19*, 15719-15725.

[145] J. Clayden, N. Greeves, S. Warren, *Organic Chemistry*, 2 ed., Oxford University Press Inc., New York, **2001**.

[146] A. Reiser, L. J. Leyshon, *Journal of the American Chemical Society* **1971**, *93*, 4051-&.

[147] W. T. Borden, N. P. Gritsan, C. M. Hadad, W. L. Karney, C. R. Kemnitz, M. S. Platz, *Accounts of Chemical Research* **2000**, *33*, 765-771.

[148] T. A. Strom, E. P. Dillon, C. E. Hamilton, A. R. Barron, *Chem Commun (Camb)* **2010**, *46*, 4097-4099.

[149] A. Faghani, I. S. Donskyi, M. Fardin Gholami, B. Ziem, A. Lippitz, W. E. Unger, C. Bottcher, J. P. Rabe, R. Haag, M. Adeli, *Angew Chem Int Ed Engl* **2017**, *56*, 2675-2679.

[150] T. Suzuki, Q. Li, K. C. Khemani, F. Wudl, O. Almarsson, *Science* **1991**, *254*, 1186-1188.

[151] F. Wudl, *Accounts of Chemical Research* **1992**, *25*, 157-161.

[152] X. Lu, F. Tian, Q. Zhang, *The Journal of Physical Chemistry B* **2003**, *107*, 8388-8391.

[153] C. K. Chua, A. Ambrosi, M. Pumera, *Chem Commun (Camb)* **2012**, *48*, 5376-5378.

[154] W. Zan, *Applied Surface Science* **2014**, *311*, 377-383.

[155] J. Park, M. Yan, *Acc Chem Res* **2013**, *46*, 181-189.

[156] X. Wang, G. Shi, *Phys Chem Chem Phys* **2015**, *17*, 28484-28504.

[157] T. Sainsbury, M. Passarelli, M. Naftaly, S. Gnaniah, S. J. Spencer, A. J. Pollard, *ACS Appl Mater Interfaces* **2016**, *8*, 4870-4877.

[158] C. R. Kemnitz, W. L. Karney, W. T. Borden, *Journal of the American Chemical Society* **1998**, *120*, 3499-3503.

[159] G. W. J. Fleet, R. R. Porter, J. R. Knowles, *Nature* **1969**, *224*, 511-512.

[160] C. J. Hawker, P. M. Saville, J. W. White, *The Journal of Organic Chemistry* **1994**, *59*, 3503-3505.

[161] S. Bahçeci Sertkol, B. Esat, A. A. Momchilov, M. Burak Yılmaz, M. Sertkol, *Carbon* **2017**, *116*, 154-166.

[162] R. Teimuri-Mofrad, R. Hadi, H. Abbasi, *J Organomet Chem* **2019**, *880*, 355-362.

[163] J. Peña-Bahamonde, V. San Miguel, H. N. Nguyen, R. Ozisik, D. F. Rodrigues, J. C. Cabanelas, *Carbon* **2017**, *111*, 258-268.

[164] Y. Yuan, P. Chen, X. Ren, H. Wang, *Chemphyschem* **2012**, *13*, 741-750.

[165] M. R. Banks, J. I. G. Cadogan, I. Gosney, P. K. G. Hodgson, P. R. R. Langridge-Smith, J. R. A. Millar, A. T. Taylor, *Tetrahedron Letters* **1994**, *35*, 9067-9070.

[166] M. Maggini, G. Scorrano, A. Bianco, C. Toniolo, R. P. Sijbesma, F. Wudl, M. Prato, *Journal of the Chemical Society, Chemical Communications* **1994**.

[167] N. Tagmatarchis, M. Prato, *Journal of Materials Chemistry* **2004**, *14*.

[168] X. Q. Wang, D. E. Jiang, S. Dai, *Chemistry of Materials* **2008**, *20*, 4800-4802.

[169] P. A. Denis, F. Iribarne, *International Journal of Quantum Chemistry* **2009**, NA-NA.

[170] X. Wu, H. Cao, B. Li, G. Yin, *Nanotechnology* **2011**, *22*, 075202.

[171] J. Choi, K.-j. Kim, B. Kim, H. Lee, S. Kim, *The Journal of Physical Chemistry C* **2009**, *113*, 9433-9435.

[172] Y. Cao, K. N. Houk, *J. Mater. Chem.* **2011**, *21*, 1503-1508.

[173] L. V. Frolova, I. V. Magedov, A. Harper, S. K. Jha, M. Ovezmyradov, G. Chandler, J. Garcia, D. Bethke, E. A. Shaner, I. Vasiliev, N. G. Kalugin, *Carbon N Y* **2015**, *81*, 216-222.

[174] M. Quintana, A. Montellano, A. E. del Rio Castillo, G. Van Tendeloo, C. Bittencourt, M. Prato, *Chem Commun (Camb)* **2011**, *47*, 9330-9332.

[175] M. K. Bayazit, S. J. A. Moniz, K. S. Coleman, *Chemical Communications* **2017**, *53*, 7748-7751.

[176] S. Sarkar, E. Bekyarova, S. Niyogi, R. C. Haddon, *J Am Chem Soc* **2011**, *133*, 3324-3327.

[177] M. A. Tasdelen, *Polymer Chemistry* **2011**, *2*, 2133.

[178] S. Sarkar, E. Bekyarova, R. C. Haddon, *Acc Chem Res* **2012**, *45*, 673-682.

[179] J. Yuan, G. Chen, W. Weng, Y. Xu, *Journal of Materials Chemistry* **2012**, *22*.

[180] S. Bian, A. M. Scott, Y. Cao, Y. Liang, S. Osuna, K. N. Houk, A. B. Braunschweig, *J Am Chem Soc* **2013**, *135*, 9240-9243.

[181] Y. Cao, S. Osuna, Y. Liang, R. C. Haddon, K. N. Houk, *J Am Chem Soc* **2013**, *135*, 17643-17649.

[182] J.-M. Seo, I.-Y. Jeon, J.-B. Baek, *Chemical Science* **2013**, *4*.

[183] P. P. Brisebois, C. Kuss, S. B. Schougaard, R. Izquierdo, M. Siaj, *Chemistry* **2016**, *22*, 5849-5852.

[184] Y. Li, F. Miomandre, G. Clavier, L. Galmiche, V. Alain-Rizzo, P. Audebert, *ChemElectroChem* **2017**, *4*, 430-435.

[185] C. Lin, D. Sheng, X. Liu, S. Xu, F. Ji, L. Dong, Y. Zhou, Y. Yang, *Polymer* **2018**, *140*, 150-157.

[186] J. Li, Q. Liu, D. Ho, S. Zhao, S. Wu, L. Ling, F. Han, X. Wu, G. Zhang, R. Sun, C.-P. Wong, *ACS Applied Materials & Interfaces* **2018**, *10*, 9727-9735.

[187] Z. Ji, J. Chen, L. Huang, G. Shi, *Chem Commun (Camb)* **2015**, *51*, 2806-2809.

[188] I.-M. Lazar, A. M. Rostas, P. S. Straub, E. Schleicher, S. Weber, R. Mülhaupt, *Macromolecular Chemistry and Physics* **2017**, *218*.

[189] M. Hammouri, S. K. Jha, I. Vasiliev, *The Journal of Physical Chemistry C* **2015**, *119*, 18719-18728.

[190] J. Li, G. Zhang, R. Sun, C.-P. Wong, *Journal of Materials Chemistry C* **2017**, *5*, 220-228.

[191] M. Fang, K. Wang, H. Lu, Y. Yang, S. Nutt, *Journal of Materials Chemistry* **2009**, *19*.

[192] M. Steenackers, A. M. Gigler, N. Zhang, F. Deubel, M. Seifert, L. H. Hess, C. H. Lim, K. P. Loh, J. A. Garrido, R. Jordan, M. Stutzmann, I. D. Sharp, *J Am Chem Soc* **2011**, *133*, 10490-10498.

[193] N. Liu, F. Luo, H. Wu, Y. Liu, C. Zhang, J. Chen, *Advanced Functional Materials* **2008**, *18*, 1518-1525.

[194] L. H. Hess, A. Lyuleeva, B. M. Blaschke, M. Sachsenhauser, M. Seifert, J. A. Garrido, F. Deubel, *ACS Appl Mater Interfaces* **2014**, *6*, 9705-9710.

[195] D. Han, P. Xiao, J. Gu, J. Chen, Z. Cai, J. Zhang, W. Wang, T. Chen, *RSC Advances* **2014**, *4*.

[196] M. Benaglia, *Recoverable and Recyclable Catalysts*, 1 ed., John Wiley & Sons, **2009**.

[197] I. T. Horvath, J. Rabai, *Science* **1994**, *266*, 72-75.

[198] B. Cornils, *Angewandte Chemie International Edition in English* **1997**, *36*, 2057-2059.

[199] E. de Wolf, G. van Koten, B.-J. Deelman, *Chemical Society Reviews* **1999**, *28*, 37-41.

[200] J. A. Gladysz, D. P. Curran, *Tetrahedron* **2002**, *58*, 3823-3825.

[201] C. C. Tzschucke, C. Markert, W. Bannwarth, S. Roller, A. Hebel, R. Haag, *Angew Chem Int Ed Engl* **2002**, *41*, 3964-4000.

[202] S. J. Tavener, J. H. Clark, *Journal of Fluorine Chemistry* **2003**, *123*, 31-36.

[203] B. Barabas, O. Fulop, R. Molontay, G. Palyi, *Acs Sustainable Chemistry & Engineering* **2017**, *5*, 8108-8118.

[204] J. M. Vincent, *Chem Commun (Camb)* **2012**, *48*, 11382-11391.

[205] J.-M. Vincent, M. Contel, G. Pozzi, R. H. Fish, *Coordination Chemistry Reviews* **2019**, *380*, 584-599.

[206] M. Wende, R. Meier, J. A. Gladysz, *Journal of the American Chemical Society* **2001**, *123*, 11490-11491.

[207] C. C. Tzschucke, C. Markert, H. Glatz, W. Bannwarth, *Angewandte Chemie-International Edition* **2002**, *41*, 4500-+.

[208] A. Garcia-Bernabe, C. C. Tzschucke, W. Bannwarth, R. Haag, *Adv Synth Catal* **2005**, *347*, 1389-1394.

[209] K. L. O'Neal, H. Zhang, Y. Yang, L. Hong, D. Lu, S. G. Weber, *J Chromatogr A* **2010**, *1217*, 2287-2295.

[210] M. Wende, J. A. Gladysz, *Journal of the American Chemical Society* **2003**, *125*, 5861-5872.

[211] C. Liu, X. Li, Z. Jin, *Catalysis Today* **2015**, *247*, 82-89.

[212] W. Zhang, in *Green Techniques for Organic Synthesis and Medicinal Chemistry*, **2018**, pp. 509-538.

[213] L. Feng, L. Wu, X. Qu, *Adv Mater* **2013**, *25*, 168-186.

[214] A. C. Ferrari, F. Bonaccorso, V. Fal'ko, K. S. Novoselov, S. Roche, P. Boggild, S. Borini, F. H. Koppens, V. Palermo, N. Pugno, J. A. Garrido, R. Sordan, A. Bianco, L. Ballerini, M. Prato, E. Lidorikis, J. Kivioja, C. Marinelli, T. Ryhanen, A. Morpurgo, J. N. Coleman, V. Nicolosi, L. Colombo, A. Fert, M. Garcia-Hernandez, A. Bachtold, G. F. Schneider, F. Guinea, C. Dekker, M. Barbone, Z. Sun, C. Galiotis, A. N. Grigorenko, G. Konstantatos, A. Kis, M. Katsnelson, L. Vandersypen, A. Loiseau, V. Morandi, D. Neumaier, E. Treossi, V. Pellegrini, M. Polini, A. Tredicucci, G. M. Williams, B. H. Hong, J. H. Ahn, J. M. Kim, H. Zirath, B. J. van Wees, H. van der Zant, L. Occhipinti, A. Di Matteo, I. A. Kinloch, T. Seyller, E. Quesnel, X. Feng, K. Teo, N. Rupesinghe, P. Hakonen, S. R. Neil, Q. Tannock, T. Lofwander, J. Kinaret, *Nanoscale* **2015**, *7*, 4598-4810.

[215] K. Yang, L. Feng, Z. Liu, *Expert Opin Drug Deliv* **2015**, *12*, 601-612.

[216] X. Xiao, Y. Li, Z. Liu, *Nat Mater* **2016**, *15*, 697-698.

[217] X. Chen, B. Wu, Y. Liu, *Chem Soc Rev* **2016**, *45*, 2057-2074.

[218] X. Li, C. W. Magnuson, A. Venugopal, R. M. Tromp, J. B. Hannon, E. M. Vogel, L. Colombo, R. S. Ruoff, *J Am Chem Soc* **2011**, *133*, 2816-2819.

[219] J. Kwak, J. H. Chu, J. K. Choi, S. D. Park, H. Go, S. Y. Kim, K. Park, S. D. Kim, Y. W. Kim, E. Yoon, S. Kodambaka, S. Y. Kwon, *Nat Commun* **2012**, *3*, 645.

[220] R. H. Fish, *Chemistry-a European Journal* **1999**, *5*, 1677-1680.

[221] H. R. Hobbs, H. M. Kirke, M. Poliakoff, N. R. Thomas, *Angew Chem Int Ed Engl* **2007**, *46*, 7860-7863.

[222] J. H. Jung, D. S. Cheon, F. Liu, K. B. Lee, T. S. Seo, *Angew Chem Int Ed Engl* **2010**, *49*, 5708-5711.

[223] F. Liu, K. S. Choi, T. J. Park, S. Y. Lee, T. S. Seo, *BioChip Journal* **2011**, *5*, 123-128.

7 Appendix

7.1 List of Publications (Journals, Posters, Patents)

1. M. Khani, E. Mehdipour, A. Faghani, **G. Guday**, I. S. Donskyi, W. E. S. Unger, R. Haag and Mohsen Adeli, *RSC Adv.*, **2016**, *6*, 115055. Preparation of graphene oxide by cyanuric chloride as an effective and non-corrosive oxidizing agent.
2. Z. Tu, **G. Guday**, M. Adeli, and Rainer Haag, *Adv. Mater.*, **2018**, *27*, 160647. Multivalent Interactions between 2D Nanomaterials and Biointerfaces.
3. Z. Tu, H. Qiao, Y. Yan, **G. Guday**, W. Chen, M. Adeli, and R. Haag, *Angew. Chem.*, **2018**, *57*, 11198-11202. Directed Graphene-Based Nanoplatforms for Hyperthermia-Overcoming Multiple Drug Resistance.
4. **G. Guday**, I. S. Donskyi, M. F. Gholami, G. Algara-Siller, F. Witte, A. Lippitz, W. E. S. Unger, B. Paulus, J. P. Rabe, M. Adeli, and R. Haag, *Small*, **2019**, *15*, 1805430. Scalable Production of Nanographene and Doping via Non-destructive Covalent Functionalization.
5. I. S. Donskyi, W. Azab, J. L. Cuellar-Camacho, **G. Guday**, A. Lippitz, W. E. S. Unger, K. Osterrieder, M. Adeli,* and R. Haag*, *Nanoscale*, **2019**, Accepted. Functionalized Nanographene Sheets with High Antiviral Activity Through Synergistic Electrostatic and Hydrophobic Interactions.
6. **G. Guday**, M. Adeli*, and R. Haag*, **2019**, Submitted. Reversible photothermal homogenization for fluorous biphasic systems with perfluoroalkylated nanographene.

Manuscripts in Preparation

1. I. S. Donskyi, H. Qiao, P. Nickl, **G. Guday**, K. Achazi, A. Lippitz, W. E. S. Unger, C. Böttcher, W. Chen,* M. Adeli,* and R. Haag, Biodegradable graphene sheets for tumor therapy.
2. **G. Guday**, I. S. Donskyi, M. Adeli, R. Haag, Graphene templated gram-scale synthesis of polyglycerol nanogels.

Conference Participation

1. **G. Guday**, M. Adeli, R. Haag
   Nanoplatforms for fluorous-phase chemistry
   GRK 1582 Symposium 2018

2. **G. Guday**, M. Adeli, R. Haag
   Mechanochemistry: Solid state functionalization of graphene
   Advances in Functional Materials 2017
3. **G. Guday,** I. S. Donskyi, M. Adeli, R. Haag
   Mild oxidative exfoliation of single-layer graphene
   Graphene2017 International Conference 2017

7.2 Curriculum Vitae

Der Lebenslauf ist aus Gründen des Datenschutzes nicht enthalten.